which is a linker region between NC and PR and lacks the PTAP motif. The defect of GagPol in particle assembly, when the GagPol contains active PR, is partly ascribed to premature processing before particle assembly by the overexpression of PR, since the overexpression of GagPol and that of the active PR dimer have been shown to result in no particle production [40–44]. While the treatment with PR inhibitors partially suppressed this defect, GagPol remained very inefficient at particle production [42], suggesting that, even when it contains inactive PR, GagPol is incapable of particle production. A very recent study investigated this possibility, revealing that the Pol region but not the p6 domain was responsible for the budding defect of GagPol [45]. However, it remains unanswered why GagPol protein is incapable of particle production. Specific questions should address at which stages and by what mechanisms the Pol region imposes the defects.

One of the difficulties in investigating GagPol trafficking is the low level of GagPol expression relative to that of Gag. Moreover, the N-terminal half of GagPol is identical to Gag, and this hinders discrimination between the two. To overcome these difficulties, we previously generated the HIV-1 molecular clone derivative containing two distinct epitope tags [FLAG and hemagglutinin (HA)] to the C-termini of Gag and GagPol, respectively [44]. The data from that study showed that both GagPol and Gag, when coexpressed, were relocated from the cytoplasm to the plasma membrane and were incorporated into viral particles, the yield of which was equivalent to that of the wild type of the HIV-1 molecular clone [44]. Using our GagPol constructs, we here address the budding defect of GagPol. Our data indicate that GagPol is originally incapable of membrane binding and that plasma membrane targeting, even when conferred, is insufficient for particle production, suggesting that other stages (e.g., multimerization) are also potentially impaired by the Pol region.

Materials and Methods

Construction of HIV-1 Molecular Clones

The derivative of HIV-1 molecular clone pNL43 containing inactive PR [46] was used as the wild type (WT) in this study. The pNL43 derivatives, Gag-FLAG/Pol-HA and GagPol-HA, both of which contain inactive PR, were described previously [44]. Briefly, the Gag-FLAG/Pol-HA expresses Gag with a C-terminal FLAG sequence and GagPol with a C-terminal HA sequence. The GagPol-HA contains a deletion of the frameshifting signal and expresses GagPol with a C-terminal HA sequence but does not express Gag. The pNL43 derivative expressing Gag-FLAG without GagPol was also described previously [44]. The pNL43 derivatives expressing truncated GagPol proteins were generated by the insertion of a premature termination codon at the junction of PR-RT and RT-IN. For the replacement of the Pol region with ß-galactosidase (ß-gal) or green fluorescent protein (GFP) in the context of the GagPol protein, unique NotI and XbaI sites were initially created at the p6*-PR junction using 5′-TTCGCGGCCGCTGCTTCTAGACCTCAGAT-CACTCTTTGGCAGCGA-3′ and 5′-AGGTCTAGAAG-CAGCGGCCGCGAAGCTAAAGGATACAGTTCCTTGT-3′ (underlined, NotI and XbaI linkers), and the ß-gal or GFP gene containing the termination codon was cloned in-frame into the NotI-XbaI junction. To generate the pNL43 derivative expressing the Gag-4GFP construct, four GFP fragments were ligated at each end using restriction sites (XbaI-BamHI-KpnI-SacI-EcoRI) and were fused with the C-terminus of Gag. GagPol constructs containing the p6 domain instead of the p6* domain were generated by the insertion of four nucleotides into the p6/p6*-PR junction (nucleotide positions 2249–2252), which placed the *gag* and *pol* genes in the same reading frame at the p6-PR junction. The C-terminal truncation of these GagPol constructs was similarly carried out by inserting a premature termination codon at the PR-RT junction. The pNL43 derivatives containing the 10 N-terminal amino acids of Fyn kinase [Fyn(10)] at the N-terminus of Gag were constructed from pNL43/Fyn(10)fullMA as described previously [47]. To create the PTAP motif within the p6* domain, the 12 nucleotides corresponding to the PTAP motif (nucleotide positions 2152 to 2163) were placed in-frame in the p6* reading frame.

Cell Culture and DNA Transfection

HeLa cells were maintained in Dulbecco's modified Eagle's medium (Sigma) supplemented with 10% fetal bovine serum. Transfection with DNA was carried out using Lipofectamine 2000 (Invitrogen).

Purification of HIV Particles

Viral particles were purified by the standard procedures. At 2 days post-transfection, culture media were clarified, filtered, and centrifuged through 20% (wt/vol) sucrose cushions in an SW55 rotor (Beckman Coulter) at 100,000×g for 2 hr at 4°C. Viral pellets were resuspended in PBS.

Membrane Flotation Centrifugation

At 2 days post-transfection, HeLa cells were harvested and resuspended in buffer containing 50 mM Tris (pH 7.5), 1 mM EDTA, 150 mM NaCl, 1 mM dithiothreitol, 1 mM phenylmethylsulfonyl fluoride, and 1 µg/ml pepstatin A. Following brief sonication, the cell lysates were clarified at 500×g for 7 min at 4°C. The supernatants were adjusted to 70% (wt/vol) sucrose, placed at the bottom of each tube, and overlaid with 65% and 10% (wt/vol) sucrose step gradients in PBS. Equilibrium flotation centrifugation was performed in an SW55 rotor at 100,000×g for 16 hr at 4°C. Fractions were collected from the bottom to the top of each tube.

Western Blot Analysis

Protein samples were subjected to sodium dodecyl sulfate-polyacrylamide gel electrophoresis (SDS-PAGE) in 10% polyacrylamide gels and were transferred to polyvinylidene difluoride membrane. The membrane was incubated with anti-HIV-1 p24 mouse antibody [48] and subsequently with horseradish peroxidase-conjugated secondary antibodies (Cappel).

Immunofluorescent Staining and Confocal Microscopy

HeLa cells were fixed with 3.7% paraformaldehyde in PBS for 30 min at room temperature and were permeabilized with 0.1% Triton X-100 for 10 min at room temperature. Following blocking with 1% bovine serum albumin in PBS, the cells were incubated with anti-HA mouse (Sigma), anti-FLAG rabbit (Sigma), or anti-HIV-1 p24 mouse [48] antibodies and subsequently with Alexa Fluor 488 or 568-conjugated antibodies (Molecular Probes). After nuclear staining with TO-PRO-3 (Molecular Probes), the cells were mounted with an antibleaching reagent and observed with a laser-scanning confocal microscope (Leica).

Metabolic Labeling

At 27 hr post-transfection, cells were metabolically labeled with [^{3}H]myristic acid (PerkinElmer) at 18.5 Mbq/ml for 3 hr. After labeling, the cells were collected and analyzed by SDS-PAGE followed by fluorography.

Electron Microscopy

HeLa cells were fixed with 2.5% glutaraldehyde in 0.1 M cacodylate buffer (pH 7.4) for 1 hr at 4°C prior to treatment with 2% osmium tetroxide for 1 hr at 4°C. Ultrathin sections were stained with uranyl acetate and lead citrate and examined with an electron microscope (H-7500, Hitachi) at 80 kV.

Results

HIV-1 GagPol and its C-terminally Truncated Derivatives are Incapable of Viral Particle Production Despite Full N-terminal Myristoylation

Previous studies have shown that expression of HIV-1 GagPol alone fails to produce viral particles [38,39]. The C-terminal truncation of GagPol still did not restore particle production ability even with high-level expression by a baculovirus system [49]. Recently, Gould's group has shown similar results in mammalian cell systems [45]. To examine the defect of HIV-1 GagPol in particle assembly, we used the PR-inactive version of pNL43 derivatives, in which the *gag* and *pol* frames were placed into the same reading frame by deleting the frameshifting signal. For positive controls, we used the pNL43 derivative expressing inactive PR without epitope tags (referred to as WT) and the pNL43 derivative expressing Gag tagged with the FLAG sequence and GagPol with the HA sequence (referred to as Gag-FLAG/Pol-HA) (Fig. 1A), both of which produced viral particles at similar levels [44]. The pNL43 derivatives with C-terminal truncation of the Pol region were made by placing a termination codon with an HA tag at each domain junction of the Pol region (Fig. 1A). HeLa cells were transfected with these GagPol constructs, and their particle production abilities were examined by Western blotting using anti-HIV-1 p24 antibody (Fig. 1B). The results confirmed that neither the full-length GagPol nor the truncated GagPol derivatives produced viral particles when expressed alone, although they were incorporated into viral particles when coexpressed with Gag-FLAG (Fig. 1B). It is well known that the production of viral particles by HIV-1 Gag protein is dependent on N-myristoylation [8,9]. To investigate the myristoylation of GagPol, HeLa cells were transfected with these GagPol constructs and were metabolically labeled with [^{3}H]myristic acid. When the [^{3}H] signals were normalized to the signals by Western blotting, the full-length GagPol and truncated GagPol proteins were found to be fully myristoylated, indicating that the budding defects of the GagPol constructs are not due to inefficient N-myristoylation (Fig. 1B, right panel).

C-terminal Truncation of GagPol Restored its Membrane Binding and Plasma Membrane Targeting

To obtain clues to the cause of the defect, we observed GagPol-HA-transfected cells by confocal microscopy. The confocal images revealed only the diffuse distribution of GagPol-HA throughout the cytoplasm (Fig. 2A). Membrane flotation analysis revealed that GagPol-HA was incapable of binding to the membrane (Fig. 2B). When the intracellular localization of the C-terminally truncated derivatives was similarly analyzed by confocal microscopy, the antigen distribution at the plasma membrane became apparent with the progressive C-terminal truncation of GagPol (Fig. 2A). Consistent with these observations, membrane flotation analysis revealed the distribution of the GagPol derivatives to membrane-bound fractions, concomitant with the progressive truncation of GagPol (Fig. 2B). Since membrane targeting of Gag/GagPol is prerequisite for type C retrovirus particle assembly, we suggest that the membrane-binding defect of GagPol is primarily responsible for the defect of full-length GagPol in particle production. However, there was no correlation between particle production (Fig. 1) and membrane binding (Fig. 2) upon C-terminal truncations, suggesting that other stages (e.g., multimerization and particle budding) are potentially impaired.

C-terminal Addition of Large Noncognate Protein to Gagp6*, Similar to the Pol Region, Reduced its Membrane Affinity

To understand GagPol's inhibitory effect on membrane binding, we replaced the Pol region with 120 kDa ß-gal and 27 kDa GFP [referred to as Gag(p6*)ß-gal and Gag(p6*)GFP, respectively]. We also made a Gag fusion construct that four tandem repeats of GFP, the length of which was nearly equivalent to the entire Pol region, were fused to the C-terminus of Gag (referred to as Gag-4GFP) (Fig. 3A). Membrane flotation analysis revealed the majorities of Gag(p6*)ß-gal and Gag-4GFP in non-membrane-bound fractions, similar to the case with GagPol-HA (Fig. 3B). In contrast, Gag(p6*)GFP was distributed to membrane-bound fractions at levels similar to those of Gag(p6*)PR-HA (compare with Fig. 2B). Confocal images were consistent with these findings, showing diffuse distribution of Gag(p6*)ß-gal and Gag-4GFP throughout the cytoplasm but, in contrast, Gag(p6*)GFP accumulation at the plasma membrane (Fig. 3C). These data suggest that the membrane-binding defect of GagPol was imposed by the C-terminal long extension, likely due to the length of the extension but not the specificity of the amino acid sequence. None of these constructs produced viral particles (Fig. 3D).

The Budding Defect of Gag(p6*)PR is not Caused by its Lack of p6 Domain

It is well known that the deletion of the PTAP motif in the Gag p6 domain blocks the pinching off of viral particles at a late stage of budding [16,18,46,50]. We reasoned that the budding defect of our constructs containing p6* might be partly due to a lack of the PTAP motif in the context of constructs, because the *gag*-to-*pol* frameshifting occurs upstream from the PTAP motif (Fig. 4A). Based on this hypothesis, we replaced the p6* with the p6 in the GagPol and Gag(p6*)PR constructs [referred to as Gag(p6)Pol and Gag(p6)PR, respectively] (Fig. 4A). As expected, membrane flotation analysis confirmed the membrane affinity of Gag(p6)PR but not that of Gag(p6)Pol (Fig. 4B). Confocal images showed antigen accumulation at the plasma membrane in Gag(p6)PR-expressing cells (Fig. 4C). However, Gag(p6)PR showed very little particle production (Fig. 4D), indicating that the p6 domain, most likely the PTAP motif, does not support efficient particle release in the case of Gag(p6)PR. A similar observation, that the budding defect of GagPol is not ascribable to the lack of p6, was reported in a very recent study [45]. These data suggested that the budding defect of Gag(p6*)PR is not due to the lack of p6 and raised the possibility that viral particle production by Gag(p6*)PR is blocked at other stages, such as Gag multimerization. We then used electron microscopy to examine this possibility (Fig. 4E). Cells expressing Gag(p6*)PR showed slightly curved, electron-dense structures at the plasma membrane but no spherical budding structures. Cells expressing Gag(p6)PR displayed aberrant morphology at the plasma membrane: some cells showed not spherical but pedestal-like electron-dense structures (5 out of 15 cells observed), distinctive from particles arrested at a late budding stage by PTAP deletion (Fig. 4E). Viral particles often displayed aberrant morphology carrying electron-dense materials (6 out of 15 cells observed). Such budding particles in an irregular shape by

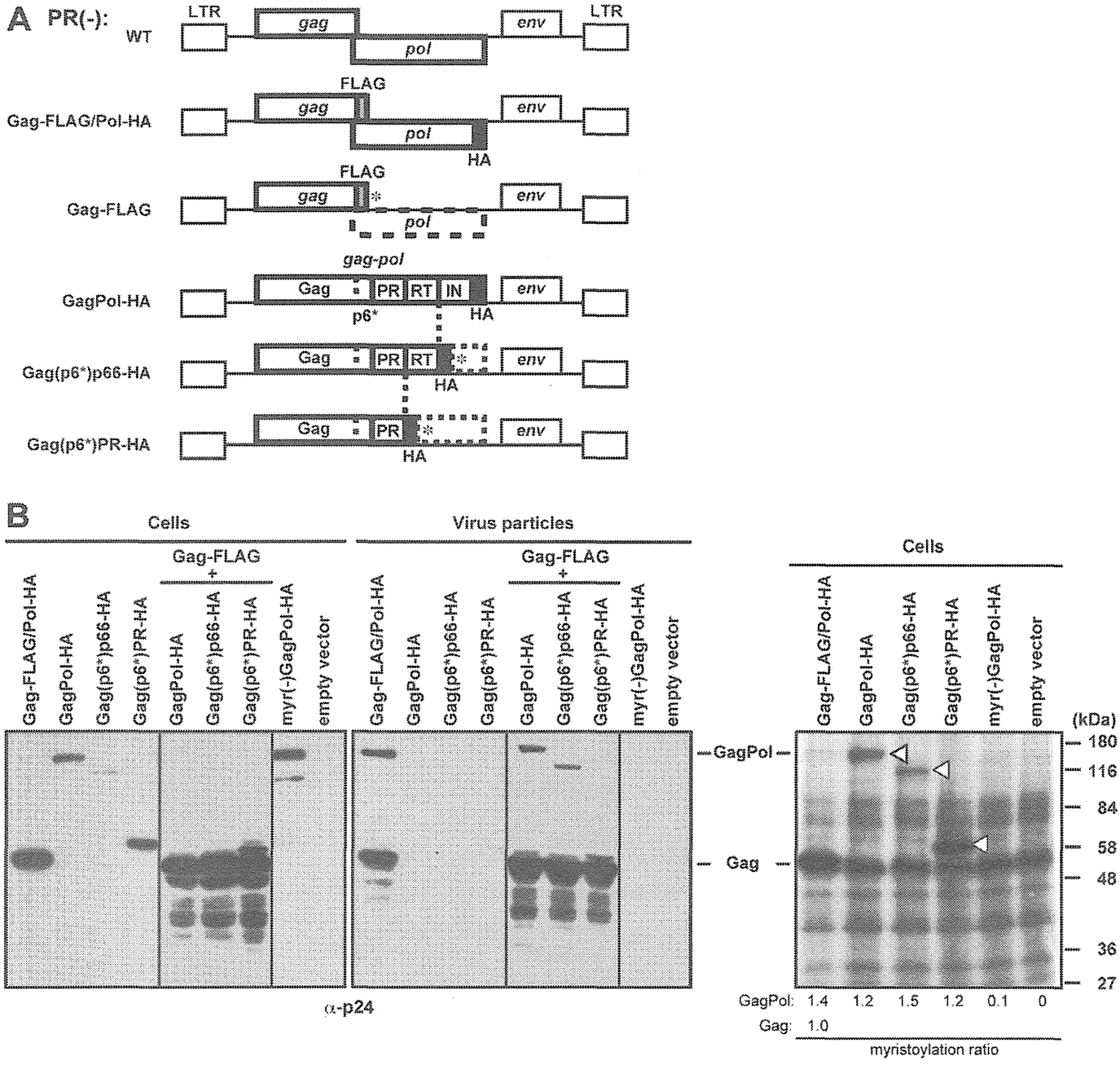

Figure 1. Viral particle production of HIV-1 GagPol and its C-terminally truncated derivatives. (A) Schematic representation of the pNL43 derivatives tagged with the FLAG and HA sequences. The pNL43 derivative containing inactive PR was used as wild type (WT). The FLAG and HA sequences were inserted in-frame in the C-terminal p6 domain of Gag and the C-terminus of GagPol, respectively (referred to as Gag-FLAG/Pol-HA) [44]. For expression of Gag-FLAG alone (without GagPol), the FLAG sequence was inserted in the C-terminal p6 domain of Gag and termination codons (asterisk) were placed in-frame in the *pol* frame. For expression of GagPol-HA (without Gag), the HA sequence was added to the C-terminus of the GagPol protein [44]. For the C-terminal truncations of GagPol, the HA sequence followed by a termination codon (asterisk) was inserted at the PR/RT or RT/IN junction of GagPol [referred to as Gag(p6*)p66-HA and Gag(p6*)PR-HA, respectively]. GagPol-HA and the derivatives contained the frameshift mutation, and all constructs contained inactive PR. LTR, long terminal repeat. (B) N-myristoylation and viral particle production of the truncated GagPol proteins. HeLa cells were singly transfected with the GagPol-HA and its C-terminally truncated constructs, or doubly transfected with a combination of the GagPol-HA and Gag-FLAG constructs at a Gag-to-GagPol DNA ratio of 1:10. Total DNA amounts were normalized to 8 μg with pUC plasmid. Gag-FLAG/Pol-HA and myr(-)GagPol-HA containing the myristoylation (G2A) mutation were used as positive and negative controls, respectively. Cells were labeled with [^{3}H]myristic acid for 3 hr and were subjected to SDS-PAGE followed by fluorography. Arrowheads indicate myristoylated GagPol-HA, Gag(p6*)p66-HA, and Gag(p6*)PR-HA, respectively. The cells and purified viral particles were subjected to Western blotting using anti-HIV-1 p24 antibody. The intensity of the band corresponding to each construct in fluorographed gels and Western blots was measured by ImageJ software. For each construct, the band intensity in fluorographed gels was divided by the band intensity in Western blots. The myristoylation ratio of Gag was set at 1.0, and the myristoylation ratios of the constructs relative to the ratio of Gag were calculated.
doi:10.1371/journal.pone.0047828.g001

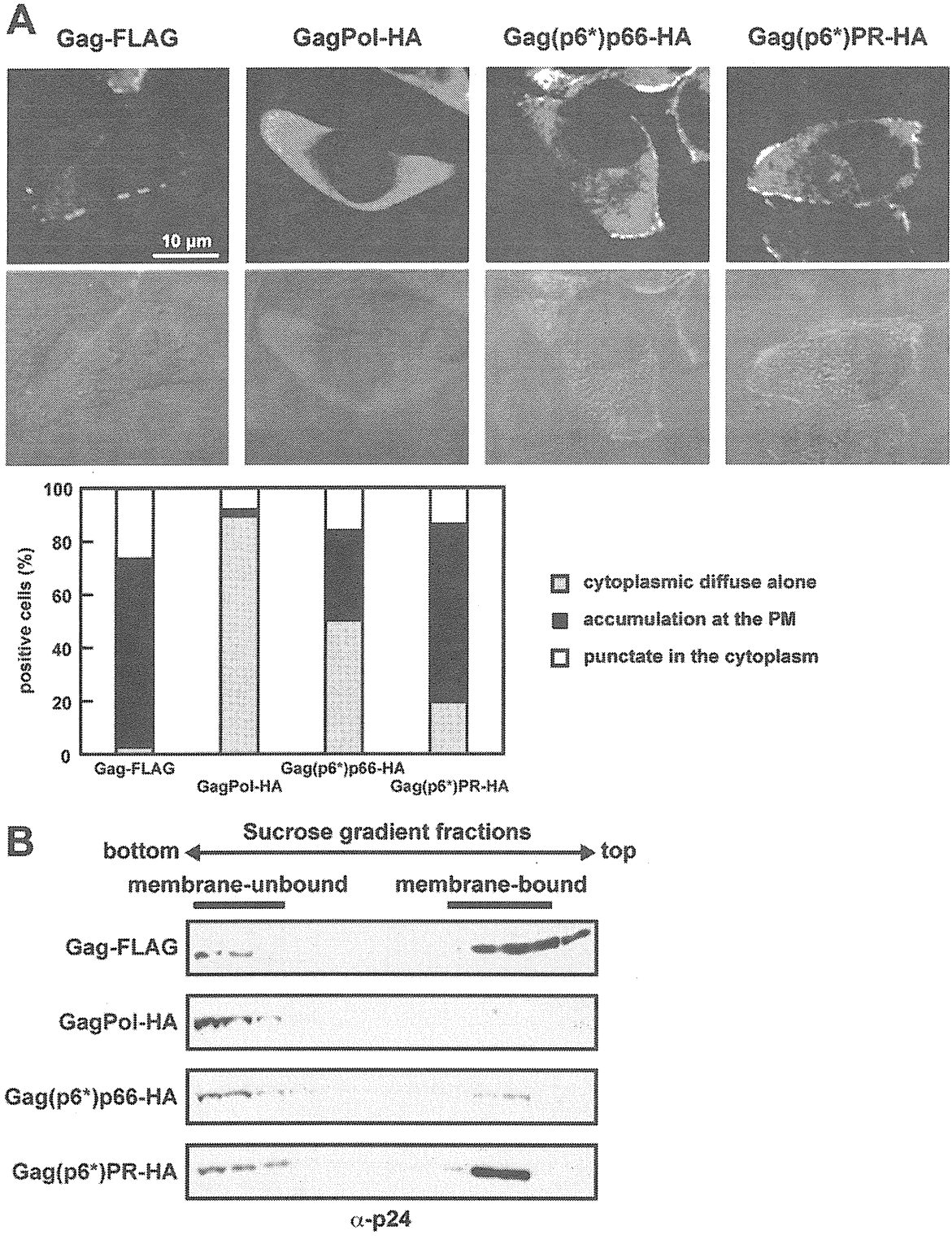

Figure 2. Membrane affinity and plasma membrane targeting of GagPol with C-terminal truncations. (A and B) HeLa cells were transfected with the Gag-FLAG, GagPol-HA, and C-terminally truncated constructs. Gag-FLAG was used as a positive control. (A) Intracellular localization of the truncated GagPol proteins. At 24 hr post-transfection, cells were immunostained with anti-FLAG (red) or anti-HA (green) antibodies and nuclei were stained with TO-PRO-3 (blue). Bottom panels show confocal images overlaid with differential interference contrast images. All micrographs are shown at the same magnification. In each sample, approximately 100 antigen-positive cells (from 3 or 4 independent experiments) were subjected to analysis of the antigen distribution pattern. (B) Membrane affinity of the truncated GagPol proteins. Cells were subjected to membrane flotation centrifugation followed by Western blotting using anti-p24 antibody. Representative blots in three independent experiments were shown.

doi:10.1371/journal.pone.0047828.g002

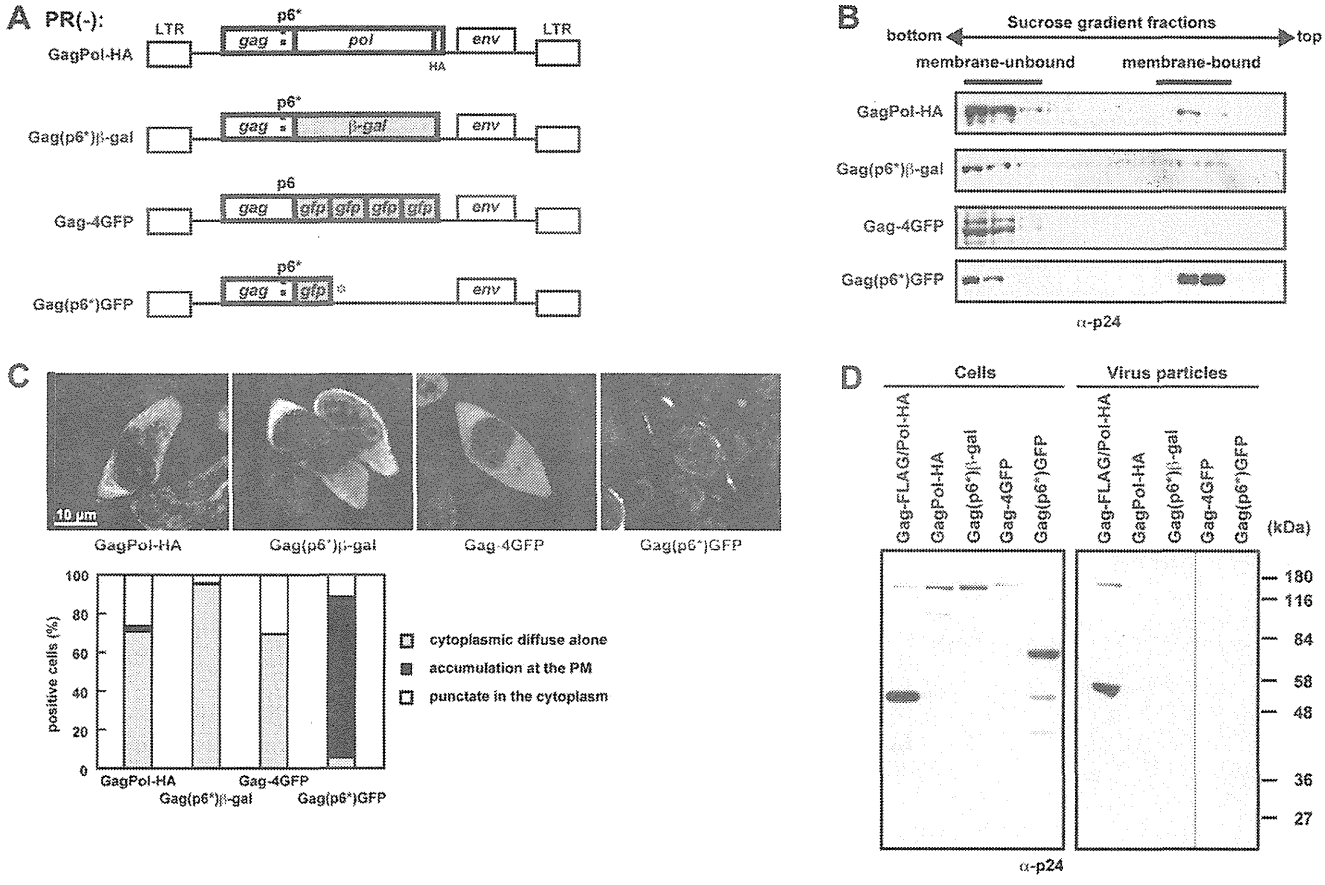

Figure 3. Membrane affinity and viral particle production of Gag with C-terminal extensions of noncognate proteins. (A) Schematic representation of the pNL43 derivatives in which the Pol region was replaced by noncognate proteins. The Pol region was replaced with ß-gal, GFP, and 4GFP [referred to as Gag(p6*)ß-gal, Gag(p6*)GFP, and Gag-4GFP, respectively]. The Gag(p6*)ß-gal and Gag(p6*)GFP contained the same frameshift mutation as described before. (B-D) HeLa cells were transfected with GagPol-HA, Gag(p6*)ß-gal, Gag(p6*)GFP, Gag-4GFP, and Gag-FLAG/Pol-HA. (B) Membrane affinity. At 24 hr post-transfection, cells were subjected to membrane flotation centrifugation followed by Western blotting using anti-p24 antibody. (C) Intracellular localization. The cells transfected with GagPol-HA or Gag(p6*)ß-gal were immunostained with anti-p24 antibody (green), and nuclei were stained with TO-PRO-3 (blue). All micrographs are shown at the same magnification. In each sample, approximately 100 antigen-positive cells (from 3 or 4 independent experiments) were subjected to analysis of their distribution patterns. (D) Intracellular expression and viral particle production. Cells and purified viral particles were subjected to Western blotting using anti-p24 antibody. Gag-FLAG/Pol-HA was used as a positive control.
doi:10.1371/journal.pone.0047828.g003

Gag(p6)PR have also been observed in insect cells [49]. These structures were not observed in untransfected cells. We speculated that the Gag construct ending at the PR domain failed to multimerize correctly at the plasma membrane during particle assembly. Alternatively, such Gag constructs may impair membrane curvature.

GagPol Failed to Produce Viral Particles Even when Recruited to the Plasma Membrane

In our study, despite N-myristoylation, GagPol protein was incapable of binding to the membrane. This raised the possibility that the presence of an N-myristoyl moiety alone was insufficient for membrane targeting in the context of GagPol. To resolve this issue, we constructed GagPol derivatives, whose initiation codons were replaced by Fyn(10) [47,51], a tight membrane-binding signal containing one myristoylation and two palmitoylation sites (Fig. 5A). The addition of the Fyn(10) signal to Gag has been shown to rescue the membrane-binding defect imposed by depletion of $PI(4,5)P_2$, a host factor that triggers the exposure of the myristoyl moiety [11,52,53]. Confocal images revealed that expression of the authentic GagPol alone showed only diffuse cytoplasmic staining. In contrast, Fyn(10)GagPol constructs were accumulated at the plasma membrane (Fig. 5B). However, Fyn(10)GagPol-HA still did not produce viral particles (Fig. 5C), and the budding defect of Fyn(10)GagPol-HA was not rescued by replacing the p6* domain with the p6 domain [referred to as Fyn(10)Gag(p6)Pol-HA] (Fig. 5C). Altogether, our data indicate that large C-terminal extension to Gag, such as the Pol region, imposes the virion release defects primarily in membrane binding and potentially in assembly.

Discussion

It has long been known that GagPol alone is incapable of viral particle production and is incorporated into viral particles only by coassembly with Gag [38,39]. Some studies on C-terminal truncation and replacement of p6* with p6 have suggested that the defect of GagPol in particle budding was not due to the lack of p6 but to the presence of the Pol region [39,45,49]. In the present study, we demonstrated that the budding defect of GagPol was

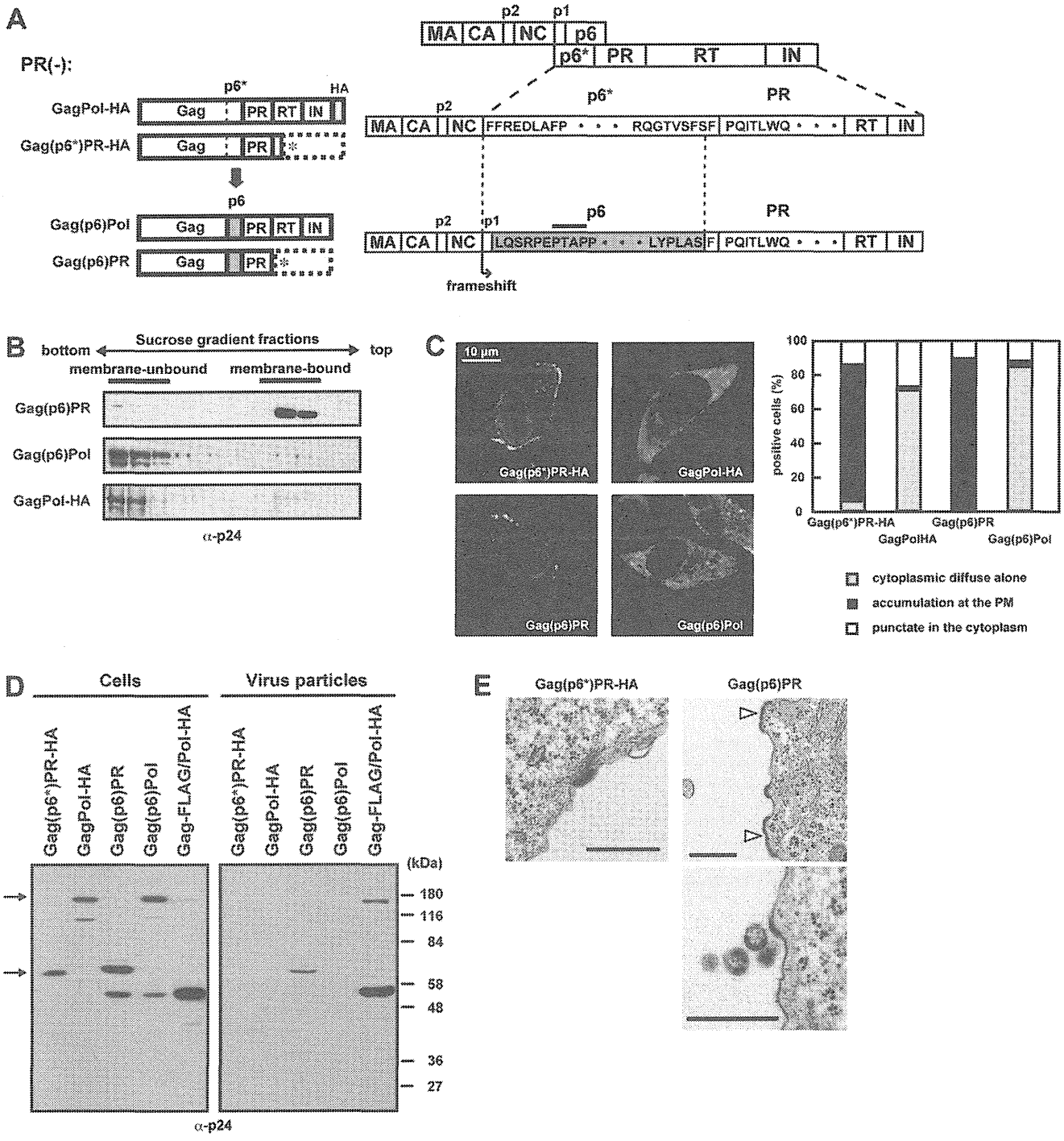

Figure 4. Viral particle production of GagPol constructs containing the p6 domain. (A) Schematic representation of the GagPol and GagPR constructs and their amino acid sequences of the p6* and p6 domains. The p6* domain was replaced by the p1+p6 domain (lacking the 12 C-terminal amino acids), and the resultant constructs were referred to as Gag(p6)Pol and Gag(p6)PR. The GagPol-HA and Gag(p6*)PR-HA constructs contain the authentic p6* domain (upper), and the Gag(p6)Pol and Gag(p6)PR constructs contain the p6 domain instead of the p6* (lower). All constructs contained inactive PR and were expressed in the context of pNL43. (B-E) HeLa cells were transfected with Gag(p6)Pol, Gag(p6)PR, GagPol-HA, and Gag(p6*)PR-HA constructs. (B) Membrane affinity of the Gag(p6)Pol and Gag(p6)PR proteins. Cells were subjected to membrane flotation centrifugation followed by Western blotting using anti-p24 antibody. (C) Intracellular localization of the Gag(p6)Pol and Gag(p6)PR proteins. Cells were immunostained with anti-p24 antibody (green), and nuclei were stained with TO-PRO-3 (blue). All micrographs are shown at the same magnification. In each sample, approximately 100 antigen-positive cells (from 3 independent experiments) were subjected to distribution pattern analysis. (D) Intracellular expression and viral particle production of the Gag(p6)Pol and Gag(p6)PR proteins. The Gag-FLAG/Pol-HA construct was used as a positive control. Cells and purified viral particles were subjected to Western blotting using anti-p24 antibody. Arrows indicate GagPol and GagPR. (E) Electron microscopy of cells transfected with Gag(p6*)PR-HA and Gag(p6)PR. The cells were stained with uranyl acetate and lead citrate. Arrowheads show pedestal-like structures. Bars, 500 nm.
doi:10.1371/journal.pone.0047828.g004

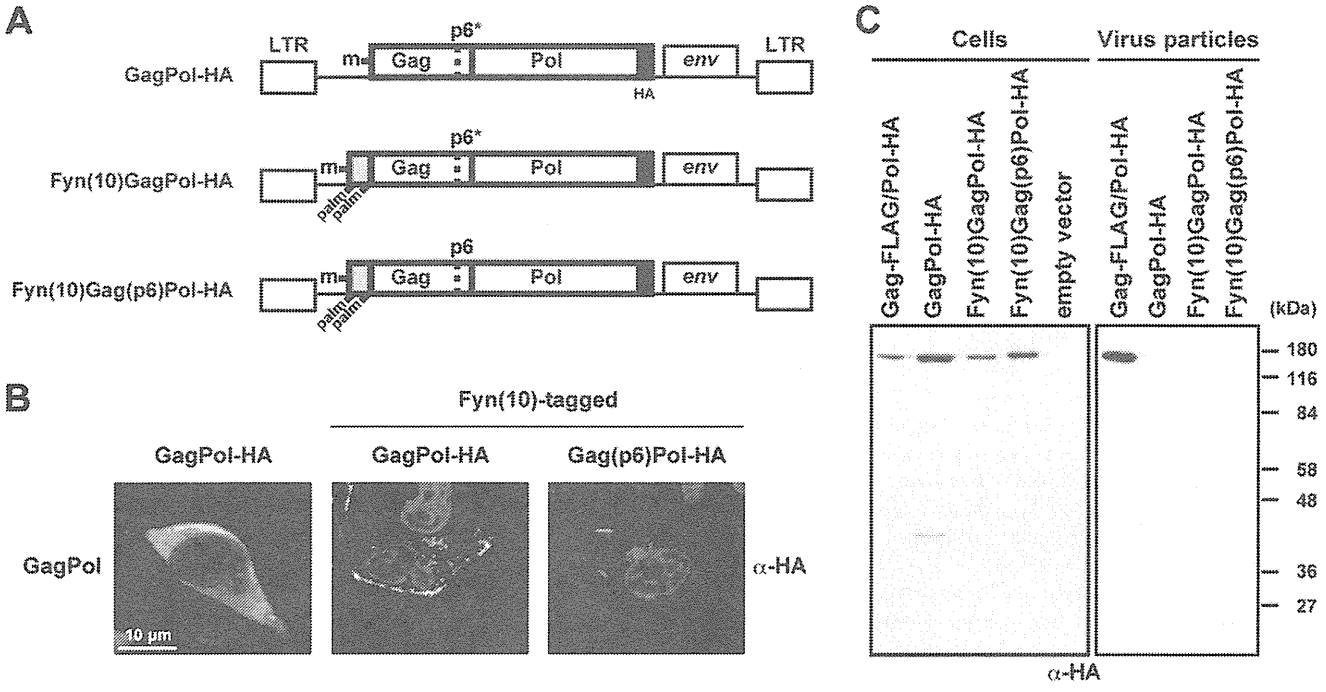

Figure 5. Plasma membrane targeting and viral particle production of GagPol with the Fyn(10) N-terminal sequence. (A) Schematic representation of GagPol-HA and its derivatives containing the Fyn(10) N-terminal sequence and the p6 domain. The initiation codon of GagPol-HA was replaced by Fyn(10) [referred to as Fyn(10)GagPol-HA] and the p6* domain was further replaced by the p6 domain [referred to as Fyn(10)Gag(p6)Pol-HA]. All constructs contained inactive PR. The letter **m** indicates a myristoylation site, and **palm** indicates a palmitoylation site. (B and C) HeLa cells were transfected with GagPol-HA, Fyn(10)GagPol-HA, and Fyn(10)Gag(p6)Pol-HA. (B) Intracellular localization of GagPol-HA derivatives. Cells were immunostained with anti-HA antibody (green or red) and nuclei were stained with TO-PRO-3 (blue). All micrographs are shown at the same magnification. (C) Intracellular expression and viral particle production. The Gag-FLAG/Pol-HA construct was used as a positive control. Cells and purified viral particles were subjected to Western blotting using anti-HA antibody.
doi:10.1371/journal.pone.0047828.g005

ascribable to the lack of membrane affinity despite full N-myristoylation.

The membrane-binding ability of Gag lies within the N-terminal MA domain that contains N-myristoylation and a cluster of basic residues, although multimerization of the CA domain has been shown to enhance the membrane binding of Gag, possibly due to the exposure of the N-terminal myristoyl moiety [5,13]. The N-terminal half of GagPol is nearly identical to Gag (MA-CA-NC), indicating that GagPol harbors all the elements supportive of its membrane binding. Nonetheless, GagPol fails to bind to the membrane. Our data, together with the previous findings, suggest the following possible explanations for the membrane-binding defect of GagPol, although alternatives cannot be ruled out. (i) The N-terminal myristoyl moiety may not be exposed in the context of GagPol. Recent NMR studies of MA have indicated that the N-terminal myristoyl moiety becomes exposed upon $PI(4,5)P_2$ binding to the basic amino acids of MA [11]. If GagPol fails to bind to $PI(4,5)P_2$, then the myristoyl moiety of GagPol may similarly remain to be occluded. Although liposome-binding assays do not allow us to provide such evidence because of limitation of GagPol detection, we found that the replacement of the authentic myristoyl signal by the Fyn(10) signal, which has been shown to rescue the Gag membrane-binding defect imposed by $PI(4,5)P_2$ depletion [53], conferred membrane-binding ability to GagPol (Fig. 5B). (ii) Alternatively, even if the myristoyl moiety is exposed, it and $PI(4,5)P_2$ binding might not suffice for stable binding to the membrane in the case of GagPol, and this would result in the rapid dissociation of GagPol from the membrane. One study has suggested that the myristoylated glycine confers 8 kcal/mol to membrane binding [54]. Recent theoretical calculations of electrostatic interactions and liposome-binding assays have indicated that monomeric HIV-1 MA has a membrane-binding energy of 5 kcal/mol [electrostatics, increasing to 7.5 kcal/mol when the membrane contains 1% $PI(4,5)P_2$] and 4 kcal/mol (myristoyl moiety, if exposed) [55–57]. This total binding energy suffices for membrane binding of Gag but may not of GagPol, since the tight membrane-binding signal Fyn(10) (containing one myristoyl and two palmitoyl moieties) was required for the membrane binding of GagPol.

Our truncation experiments indicated that the membrane affinity of GagPol was recovered upon progressive C-terminal truncation of the Pol region (Fig. 2B). The truncated constructs showed no particle production [in the case of Gag(p6*)p66-HA] or very little particle production [in the case of Gag(p6*)PR-HA] (Fig. 1B). Similar observations, e.g., the more progressive the Pol truncation, the less defective Pol is for particle formation, have been reported, although the extent of particle production by GagPR varied in different cell systems (293T and insect cells) [45,49]. These studies also indicated that GagPRRT failed to produce viral particles by electron microscopic analysis [49] and by Western blotting of the particle fractions [45]. The latter study suggested that the RT region was responsible for the defect of GagPol particle budding. Our study made similar observations but revealed by membrane flotation analysis that the budding defects were linked with no or little membrane-binding ability in the case of Gag(p6*)p66 and GagPol (Fig. 2B). More importantly, our substitution experiments clearly show that membrane binding is also impaired if the Pol region is replaced by a noncognate large

protein (e.g., ß-gal, 4GFP) (Fig. 3B). Although we cannot exclude a possibility that ß-gal and 4GFP may aggregate as dimers or oligomers and impair the membrane-binding ability, at least, our data indicate that the budding defect observed for GagPol is not caused by the RT sequence. It remains to be elucidated why C-terminal long extensions to Gag impair the membrane binding of Gag. Recent studies have suggested that the basic clusters present in the MA and NC domains both bind to RNA and fold Gag into a compact structure [58,59] but that the RNA on the MA basic cluster gets displaced by $PI(4,5)P_2$ enriched at the plasma membrane [60,61], possibly allowing Gag to stretch out to stimulate its multimerization. Although little is known about the GagPol-RNA-membrane interactions, one report has shown that RNA does not bind to the NC domain within GagPol but facilitates Gag-GagPol interactions [62]. These studies suggest a possibility that the RNA bound to Gag also binds to the MA domain of GagPol. It is tempting to speculate that GagPol alone lacks the membrane-binding ability because its MA domain is masked by RNA but the RNA-mediated Gag-GagPol interactions can bring GagPol to the plasma membrane.

It is well known that the deletion of the PTAP motif or the p6 domain from Gag arrests particle budding at a late stage, showing viral particles tethered to the plasma membrane. In our study, however, even though Gag(p6*)PR-HA accumulated at the plasma membrane, it did not show particle-like structures. The Gag(p6)PR construct, despite having the p6 domain, did not produce spherical budding particles (Fig. 4E). These data raise the possibility that the PR domain at least in the context of GagPR might inhibit correct assembly and/or membrane curvature at an early step of particle budding. The aberration of particle assembly by the presence of C-terminal PR has been observed for HIV-1 in insect cells [49]. Rous sarcoma virus Gag protein naturally includes the PR domain at its C-terminus and produces virus particles in avian and mammalian cells, but insect cells it showed virion assembly defect, which was rescued by deletion of the PR domain [63]. Although we still do not understand exactly how HIV-1 Pol impairs Gag membrane binding or how PR impairs Gag assembly, our observations in this study provide important clues toward a full understanding of the budding defect of retroviral GagPol.

Acknowledgments

We thank A. Ono and Y. Tsunetsugu-Yokota for supply of pNL43/Fyn(10)fullMA and anti-HIV-1 p24 mouse antibody, respectively.

Author Contributions

Conceived and designed the experiments: YM. Performed the experiments: HH TN. Analyzed the data: HH YM. Contributed reagents/materials/analysis tools: HH TN YK YM. Wrote the paper: HH YM.

References

1. Jacks T, Power MD, Masiarz FR, Luciw PA, Barr PJ, et al. (1988) Characterization of ribosomal frameshifting in HIV-1 gag-pol expression. Nature 331: 280–283.
2. Wilson W, Braddock M, Adams SE, Rathjen PD, Kingsman SM, et al. (1988) HIV expression strategies: ribosomal frameshifting is directed by a short sequence in both mammalian and yeast systems. Cell 55: 1159–1169.
3. Campbell S, Vogt VM (1995) Self-assembly in vitro of purified CA-NC proteins from Rous sarcoma virus and human immunodeficiency virus type 1. J Virol 69: 6487–6497.
4. Gamble TR, Yoo S, Vajdos FF, von Schwedler UK, Worthylake DK, et al. (1997) Structure of the carboxyl-terminal dimerization domain of the HIV-1 capsid protein. Science 278: 849–853.
5. Sandefur S, Varthakavi V, Spearman P (1998) The I domain is required for efficient plasma membrane binding of human immunodeficiency virus type 1 Pr55Gag. J Virol 72: 2723–2732.
6. Campbell S, Rein A (1999) In vitro assembly properties of human immunodeficiency virus type 1 Gag protein lacking the p6 domain. J Virol 73: 2270–2279.
7. Li S, Hill CP, Sundquist WI, Finch JT (2000) Image reconstructions of helical assemblies of the HIV-1 CA protein. Nature 407: 409–413.
8. Gottlinger HG, Sodroski JG, Haseltine WA (1989) Role of capsid precursor processing and myristoylation in morphogenesis and infectivity of human immunodeficiency virus type 1. Proc Natl Acad Sci U S A 86: 5781–5785.
9. Bryant M, Ratner L (1990) Myristoylation-dependent replication and assembly of human immunodeficiency virus 1. Proc Natl Acad Sci U S A 87: 523–527.
10. Zhou W, Parent LJ, Wills JW, Resh MD (1994) Identification of a membrane-binding domain within the amino-terminal region of human immunodeficiency virus type 1 Gag protein which interacts with acidic phospholipids. J Virol 68: 2556–2569.
11. Saad JS, Miller J, Tai J, Kim A, Ghanam RH, et al. (2006) Structural basis for targeting HIV-1 Gag proteins to the plasma membrane for virus assembly. Proc Natl Acad Sci U S A 103: 11364–11369.
12. Ono A, Demirov D, Freed EO (2000) Relationship between human immunodeficiency virus type 1 Gag multimerization and membrane binding. J Virol 74: 5142–5150.
13. Tang C, Loeliger E, Luncsford P, Kinde I, Beckett D, et al. (2004) Entropic switch regulates myristate exposure in the HIV-1 matrix protein. Proc Natl Acad Sci U S A 101: 517–522.
14. Li H, Dou J, Ding L, Spearman P (2007) Myristoylation is required for human immunodeficiency virus type 1 Gag-Gag multimerization in mammalian cells. J Virol 81: 12899–12910.
15. Hogue IB, Hoppe A, Ono A (2009) Quantitative fluorescence resonance energy transfer microscopy analysis of the human immunodeficiency virus type 1 Gag-Gag interaction: relative contributions of the CA and NC domains and membrane binding. J Virol 83: 7322–7336.
16. von Schwedler UK, Stuchell M, Muller B, Ward DM, Chung HY, et al. (2003) The protein network of HIV budding. Cell 114: 701–713.
17. Demirov DG, Freed EO (2004) Retrovirus budding. Virus Res 106: 87–102.
18. Garrus JE, von Schwedler UK, Pornillos OW, Morham SG, Zavitz KH, et al. (2001) Tsg101 and the vacuolar protein sorting pathway are essential for HIV-1 budding. Cell 107: 55–65.
19. VerPlank L, Bouamr F, LaGrassa TJ, Agresta B, Kikonyogo A, et al. (2001) Tsg101, a homologue of ubiquitin-conjugating (E2) enzymes, binds the L domain in HIV type 1 Pr55(Gag). Proc Natl Acad Sci U S A 98: 7724–7729.
20. Demirov DG, Ono A, Orenstein JM, Freed EO (2002) Overexpression of the N-terminal domain of TSG101 inhibits HIV-1 budding by blocking late domain function. Proc Natl Acad Sci U S A 99: 955–960.
21. Martin-Serrano J, Zang T, Bieniasz PD (2003) Role of ESCRT-I in Retroviral Budding. J Virol 77: 4794–4804.
22. Jouvenet N, Neil SJ, Bess C, Johnson MC, Virgen CA, et al. (2006) Plasma membrane is the site of productive HIV-1 particle assembly. PLoS Biol 4: e435.
23. Nydegger S, Khurana S, Krementsov DN, Foti M, Thali M (2006) Mapping of tetraspanin-enriched microdomains that can function as gateways for HIV-1. J Cell Biol 173: 795–807.
24. Deneka M, Pelchen-Matthews A, Byland R, Ruiz-Mateos E, Marsh M (2007) In macrophages, HIV-1 assembles into an intracellular plasma membrane domain containing the tetraspanins CD81, CD9, and CD53. J Cell Biol 177; 329–341.
25. Finzi A, Orthwein A, Mercier J, Cohen EA (2007) Productive Human Immunodeficiency Virus Type 1 Assembly Takes Place at the Plasma Membrane. J Virol 81: 7476–7490.
26. Jouvenet N, Bieniasz PD, Simon SM (2008) Imaging the biogenesis of individual HIV-1 virions in live cells. Nature 454: 236–240.
27. Raposo G, Moore M, Innes D, Leijendekker R, Leigh-Brown A, et al. (2002) Human macrophages accumulate HIV-1 particles in MHC II compartments. Traffic 3: 718–729.
28. Nguyen DG, Booth A, Gould SJ, Hildreth JE (2003) Evidence That HIV Budding in Primary Macrophages Occurs through the Exosome Release Pathway. J Biol Chem 278: 52347–52354.
29. Nydegger S, Foti M, Derdowski A, Spearman P, Thali M (2003) HIV-1 egress is gated through late endosomal membranes. Traffic 4: 902–910.
30. Pelchen-Matthews A, Kramer B, Marsh M (2003) Infectious HIV-1 assembles in late endosomes in primary macrophages. J Cell Biol 162: 443–455.
31. Sherer NM, Lehmann MJ, Jimenez-Soto LF, Ingmundson A, Horner SM, et al. (2003) Visualization of retroviral replication in living cells reveals budding into multivesicular bodies. Traffic 4: 785–801.
32. Grigorov B, Arcanger F, Roingeard P, Darlix JL, Muriaux D (2006) Assembly of infectious HIV-1 in human epithelial and T-lymphoblastic cell lines. J Mol Biol 359: 848–862.
33. Perlman M, Resh MD (2006) Identification of an intracellular trafficking and assembly pathway for HIV-1 Gag. Traffic 7: 731–745.
34. Jouve M, Sol-Foulon N, Watson S, Schwartz O, Benaroch P (2007) HIV-1 buds and accumulates in "nonacidic" endosomes of macrophages. Cell Host Microbe 2: 85–95.
35. Felsenstein KM, Goff SP (1988) Expression of the gag-pol fusion protein of Moloney murine leukemia virus without gag protein does not induce virion formation or proteolytic processing. J Virol 62: 2179–2182.

36. Weaver TA, Talbot KJ, Panganiban AT (1990) Spleen necrosis virus gag polyprotein is necessary for particle assembly and release but not for proteolytic processing. J Virol 64: 2642–2652.
37. Bennett RP, Rhee S, Craven RC, Hunter E, Wills JW (1991) Amino acids encoded downstream of gag are not required by Rous sarcoma virus protease during gag-mediated assembly. J Virol 65: 272–280.
38. Park J, Morrow CD (1992) The nonmyristylated $Pr160^{gag\text{-}pol}$ polyprotein of human immunodeficiency virus type 1 interacts with $Pr55^{gag}$ and is incorporated into viruslike particles. J Virol 66: 6304–6313.
39. Smith AJ, Srinivasakumar N, Hammarskjold ML, Rekosh D (1993) Requirements for incorporation of $Pr160^{gag\text{-}pol}$ from human immunodeficiency virus type 1 into virus-like particles. J Virol 67: 2266–2275.
40. Krausslich HG (1991) Human immunodeficiency virus proteinase dimer as component of the viral polyprotein prevents particle assembly and viral infectivity. Proc Natl Acad Sci U S A 88: 3213–3217.
41. Park J, Morrow CD (1991) Overexpression of the gag-pol precursor from human immunodeficiency virus type 1 proviral genomes results in efficient proteolytic processing in the absence of virion production. J Virol 65: 5111–5117.
42. Karacostas V, Wolffe EJ, Nagashima K, Gonda MA, Moss B (1993) Overexpression of the HIV-1 *gag-pol* polyprotein results in intracellular activation of HIV-1 protease and inhibition of assembly and budding of virus-like particles. Virology 193: 661–671.
43. Shehu-Xhilaga M, Crowe SM, Mak J (2001) Maintenance of the Gag/Gag-Pol ratio is important for human immunodeficiency virus type 1 RNA dimerization and viral infectivity. J Virol 75: 1834–41.
44. Haraguchi H, Sudo S, Noda T, Momose F, Kawaoka Y, et al. (2010) Intracellular localization of human immunodeficiency virus type 1 Gag and GagPol products and virus particle release: relationship with the Gag-to-GagPol ratio. Microbiol Immunol 54: 734–746.
45. Gan X, Gould SJ (2012) HIV Pol inhibits HIV budding and mediates the severe budding defect of Gag-Pol. PLoS One 7: e29421.
46. Huang M, Orenstein JM, Martin MA, Freed EO (1995) p6Gag is required for particle production from full-length human immunodeficiency virus type 1 molecular clones expressing protease. J Virol 69: 6810–6818.
47. Ono A, Waheed AA, Freed EO (2007) Depletion of cellular cholesterol inhibits membrane binding and higher-order multimerization of human immunodeficiency virus type 1 Gag. Virology 360: 27–35.
48. Tsunetsugu-Yokota Y, Ishige M, Murakami M (2007) Oral attenuated Salmonella enterica serovar Typhimurium vaccine expressing codon-optimized HIV type 1 Gag enhanced intestinal immunity in mice. AIDS Res. Hum. Retroviruses. 23: 278–286.
49. Royer M, Bardy M, Gay B, Tournier J, Boulanger P (1997) Proteolytic activity in vivo and encapsidation of recombinant human immunodeficiency virus type 1 proteinase expressed in baculovirus-infected cells. J Gen Virol 78: 131–42.
50. Gottlinger HG, Dorfman T, Sodroski JG, Haseltine WA (1991) Effect of mutations affecting the p6 gag protein on human immunodeficiency virus particle release. Proc Natl Acad Sci U S A 88: 3195–3199.
51. Lindwasser OW, Resh MD (2001) Multimerization of human immunodeficiency virus type 1 Gag promotes its localization to barges, raft-like membrane microdomains. J Virol 75: 7913–7924.
52. Saad JS, Loeliger E, Luncsford P, Liriano M, Tai J, et al. (2007) Point mutations in the HIV-1 matrix protein turn off the myristyl switch. J Mol Biol 366: 574–585.
53. Chukkapalli V, Hogue IB, Boyko V, Hu WS, Ono A (2008) Interaction between the human immunodeficiency virus type 1 Gag matrix domain and phosphatidylinositol-(4,5)-bisphosphate is essential for efficient gag membrane binding. J Virol 82: 2405–2417.
54. Peitzsch RM, McLaughlin S (1993) Binding of acylated peptides and fatty acids to phospholipid vesicles: pertinence to myristoylated proteins. Biochemistry 32: 10436–10443.
55. Murray PS, Li Z, Wang J, Tang CL, Honig B, et al. (2005) Retroviral matrix domains share electrostatic homology: models for membrane binding function throughout the viral life cycle. Structure 13: 1521–1531.
56. Mulgrew-Nesbitt A, Diraviyam K, Wang J, Singh S, Murray P, et al. (2006) The role of electrostatics in protein-membrane interactions. Biochim Biophys Acta 1761: 812–826.
57. Dalton AK, Ako-Adjei D, Murray PS, Murray D, Vogt VM (2007) Electrostatic interactions drive membrane association of the human immunodeficiency virus type 1 Gag MA domain. J Virol 81: 6434–6445.
58. Datta SA, Curtis JE, Ratcliff W, Clark PK, Crist RM, et al. (2007) Conformation of the HIV-1 Gag protein in solution. J Mol Biol 365: 812–824.
59. Datta SA, Heinrich F, Raghunandan S, Krueger S, Curtis JE, et al. (2011) HIV-1 Gag extension: conformational changes require simultaneous interaction with membrane and nucleic acid. J Mol Biol 406: 205–214.
60. Alfadhli A, Still A, Barklis E (2009) Analysis of human immunodeficiency virus type 1 matrix binding to membranes and nucleic acids. J Virol 83: 12196–12203.
61. Chukkapalli V, Oh SJ, Ono A (2010) Opposing mechanisms involving RNA and lipids regulate HIV-1 Gag membrane binding through the highly basic region of the matrix domain. Proc Natl Acad Sci U S A 107: 1600–1605.
62. Khorchid A, Halwani R, Wainberg MA, Kleiman L (2002) Role of RNA in facilitating Gag/Gag-Pol interaction. J Virol 76: 4131–4137.
63. Johnson MC, Scobie HM, Vogt VM (2001) PR domain of Rous sarcoma virus Gag causes an assembly/budding defect in insect cells. J Virol 75: 4407–4412.

SCIENTIFIC REPORTS

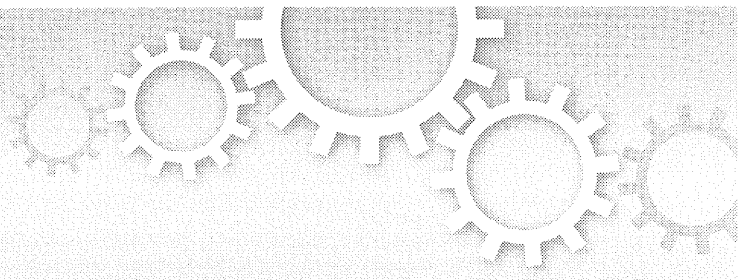

SUBJECT AREAS:
CANCER GENOMICS
HAEMATOLOGICAL CANCER
DNA DAMAGE AND REPAIR
ONCOGENES

Received
2 August 2012

Accepted
10 October 2012

Published
13 November 2012

Correspondence and requests for materials should be addressed to K.S. (shind009@kuhp.kyoto-u.ac.jp)

APOBEC3B can impair genomic stability by inducing base substitutions in genomic DNA in human cells

Masanobu Shinohara, Katsuhiro Io, Keisuke Shindo, Masashi Matsui, Takashi Sakamoto, Kohei Tada, Masayuki Kobayashi, Norimitsu Kadowaki & Akifumi Takaori-Kondo

Department of Hematology and Oncology, Graduate school of medicine, Kyoto University, Kyoto 606-8507, Japan.

Human APOBEC3 proteins play pivotal roles in intracellular defense against viral infection by catalyzing deamination of cytidine residues, leading to base substitutions in viral DNA. Activation-induced cytidine deaminase (AID), another member of the APOBEC family, is capable of editing immunoglobulin (Ig) and non-Ig genes, and aberrant expression of AID leads to tumorigenesis. However, it remains unclear whether APOBEC3 (A3) proteins affect stability of human genome. Here we demonstrate that both A3A and A3B can induce base substitutions into human genome as AID can. A3B is highly expressed in several lymphoma cells and somatic mutations occur in some oncogenes of the cells highly expressing A3B. Furthermore, transfection of *A3B* gene into lymphoma cells induces base substitutions in *cMYC* gene. These data suggest that aberrant expression of A3B can evoke genomic instability by inducing base substitutions into human genome, which might lead to tumorigenesis in human cells.

It is widely recognized that the accumulation of genetic changes in tumor-related genes is essential for cancer development[1]. With the innovation of high-throughput sequencing technology, genome-wide analyses on various types of cancer cells have revealed numerous somatic mutations in tumor-related genes[2]. Some of these mutations are caused by defects in DNA repair systems (e.g., DNA mismatch repair deficiencies give rise to hereditary non-polyposis colon cancer[3]), whereas mechanisms that account for the majority of genetic changes in cancer cells are poorly understood. Referring to somatic base substitution spectra in cancer cells, C/G to T/A transitions are most prevalent, especially in gastric cancer, colorectal cancer, glioma, and melanoma[2,4,5]. This strong bias in somatic mutations suggests the existence of active mechanisms that induce C/G to T/A transitions into genomic DNA. It is obviously attributable to ultraviolet irradiation and following repair process against pyrimidine dimer in case of melanoma, but not in others.

The human APOBEC family proteins can induce C to T (G to A, in complementary sequences) transitions into target DNA through cytidine deamination. The APOBEC family is comprised of a series of molecules with conserved cytidine deaminase domains (CDAs), including AID, APOBEC1, APOBEC2, APOBEC3A to H, and APOBEC4[6,7]. Among them, AID plays a crucial role in somatic hypermutation and class switch recombination of Ig genes, which enables diversification of immune system[8]. AID has been considered the only molecule that can induce C/G to T/A transitions into genomic DNA. The expression of AID is highly regulated and restricted in germinal center B-cells under physiological conditions, but with inflammatory stimulations, AID can be overexpressed in not only B-cells but also other types of cells (e.g., epithelial cells) via activation of NF-κB[9]. Aberrant expression of AID results in the accumulation of mutations in non-Ig genes[10], which leads to development of various cancers such as gastric and hepatic cancers as well as lymphomas[9,11–13].

A series of seven A3 genes are tandemly arrayed on human chromosome 22, and the main function of the resulting gene products is to protect the cells from retroviruses and endogenous mobile retroelements[14,15]. A3B, A3D, A3F, and A3G contain two CDAs, instead of one in A3A, A3C, and A3H. A3G is a powerful anti-retroviral molecule that induces cytidine deamination in viral genome and acts as a host defensive factor against viruses such as HIV-1[16]. A3A and A3B have been reported as potent inhibitors of retrotransposons[17]. Thus, A3 proteins act as sentinels in innate immunity against mobile DNA/RNA including viruses, while little is known about the effect of these proteins on nuclear DNA, in other words, host human genome. Recent studies have demonstrated that A3A impairs nuclear DNA under the condition of suppressing uracil DNA-glycosylase (UNG) which prevents base alterations by eliminating uracil from DNA and initiating the base-excision repair pathway[18,19].

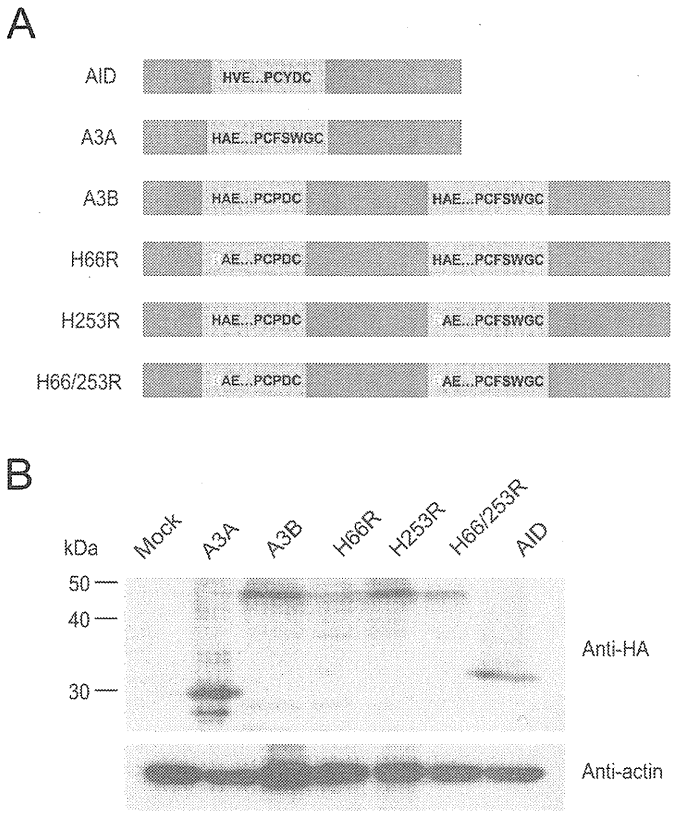

Figure 1 | Expression of A3A, A3B wild-type and mutants, and AID. (A) Schematic of expression vectors. The consensus amino acid residues for zinc-coordinating motifs are shown. Substituted residues are shown in white. (B) Expression of HA-tagged proteins. Expression vectors were transfected into HEK293 cells, and cell lysates were analyzed by immunoblotting with anti-HA antibody (top panel) and anti-ß-actin antibody (bottom panel) for loading control.

However, it is still unclear whether A3 proteins can induce somatic mutations into human genome with intact DNA repair systems. Here we first demonstrate that expression of A3B and A3A as well as AID can induce somatic mutations in genomic DNA in human cells even in the presence of UNG. We also find that high expression of A3B leads to somatic mutations in tumor-related genes. These data suggest that aberrant expression of A3B might be one of the active mechanisms that induce somatic mutations in cancer cells.

Results

A3 and AID induce hypermutations into foreign DNA. Besides A3A, we focused on A3B because it is localized predominantly in the nucleus[20,21] and highly expressed in many types of cancer cells[14] referring to microarray database (e.g., NextBio: http://www.nextbio.com). Previous studies have shown that A3B contains two enzymatically active CDAs in restricting HIV-1[22], whereas only carboxyl-terminal CDA is responsible for inhibiting HBV replication[23,24] and editing bacterial DNA[22]. A3B is also shown to restrict foreign DNA in mammalian cells[25], but it has not been tested which CDA is active in this context. First, to examine whether A3 and AID induce mutations in foreign DNA in human cells and which CDA is responsible for this DNA editing, we constructed amino- and/or carboxyl-terminal CDA mutants (H66R, H253R, and H66/253R) by site directed mutagenesis (Fig. 1a) and confirmed their expression in HEK293 cells by immunoblotting (Fig 1b). We transfected expression vectors for these together with EGFP expression vector into HEK293 cells and examined base substitutions in *EGFP* sequences. The expression vector for UNG inhibitor (UGI) was also co-transfected to avoid UNG-triggered degradation of uracil-containing foreign DNA as described previously[25]. We recovered total DNA from the cells 2 days after transfection and performed differential DNA denaturation PCR (3D-PCR) to efficiently recover edited DNA sequences[26]. 3D-PCR is based on the principle that DNA sequences with fewer interstrand hydrogen bonds dissociates easier. If cytidine deamination takes place frequently, resulting AT-rich *EGFP* gene can be amplified at lower denaturation temperatures. Although PCR products were obtained from all samples at 92°C of denaturation temperature (Td), we obtained robust PCR products at 83.8°C of Td only from A3A-, A3B wild-type (WT)-, and AID-expressing cells (Fig 2a). Amplification of *EGFP* at the lowest Td was impaired in H66R-expressing cells compared to A3B WT-expressing cells and undetectable in H253R- or H66/253R-expressing cells (Fig 2a, bottom). To ascertain whether *EGFP* gene was actually hyperedited, we cloned and sequenced the amplicons at 83.8°C of Td. As can be seen from the mutation matrices, high levels of C/G to T/A transitions were introduced into *EGFP* sequences (Fig 2b). To compare the extent of baseline mutations and that of A3B-induced mutations, we also cloned and sequenced the amplicons at 94.0°C of Td. Mutation frequency of A3B-expressing cells were about 6 times higher than that of mock-transfected cells (Supplementary Fig. S1 online). The mutation frequency in H66R-expressing cells was approximately a half compared to that in A3B WT-expressing cells in the amplicons at the lowest Td (Fig 2c). These data suggest that carboxyl-terminal CDA of A3B is mainly responsible for foreign DNA editing, but both domains are requisite for full editing activity. It is worth noting that AID is also capable of inducing cytidine deamination into foreign DNA.

Human A3 proteins have preferred target dinucleotide sequences in the substrate DNA; A3A and A3B prefer to deaminate cytosine residues flanked by 5′ thymine residue, 5′-TC, whereas A3G prefers to deaminate cytosine residues flanked by 5′ cytosine residue, 5′-CC[25,27–29]. We analyzed the context of C/G to T/A transitions in hyperedited *EGFP* sequences. We observed a strong bias toward deamination at 5′-TC dinucleotides in A3A-, A3B WT-, and H66R-expressing cells, but not in AID-expressing cells (Fig 2d). 5′-TC dinucleotide preference of A3B was also confirmed by sequencing amplicon at 94.0°C of Td which is supposed to be unbiased (Supplementary Fig. S1 online). These data suggest that the preference of editing sites in foreign DNA by A3s coincides with that seen in viral DNA.

A3A and A3B can edit genomic DNA in human cells. We next investigated whether A3 proteins induce C/G to T/A transitions into not only foreign DNA but also nuclear DNA in human cells. We first established a HEK293 cell line stably expressing EGFP (HEK293/EGFP) using retrovirus vector that carries *EGFP*. We transfected HEK293/EGFP cells with expression vectors for A3A, A3B WT or mutant (H66R, H253R, or H66/253R), or AID by lipofection, and then recovered total DNA from these cells after 7-day culture. We performed 3D-PCR of *EGFP* gene and obtained amplicons from A3A-, A3B WT-, H66R-, and AID-expressing cells at lower Td (Fig 3a). *EGFP* gene was recovered at Td as low as 86.3°C from A3B WT-expressing cells, while as low as 86.5°C from A3A-, H66R-, and AID-expressing cells. By contrast, *EGFP* gene was not amplified below Td of 87°C from cells transfected with mock, H253R or H66/253R. We repeated this procedure consisting of transfection, DNA extraction, and 3D-PCR three times and obtained similar results (Fig 3b). To unambiguously confirm the presence of C/G to T/A transitions, we cloned and sequenced amplicons obtained at the lowest Td in A3A-, A3B WT-, H66R-, and AID-expressing cells (Fig 3c). These analyses revealed approximately 2 to 5 C/G to T/A transitions per *EGFP* sequence from each sample (Fig 3d). The transitions were detected most frequently in A3A-expressing cells, and deaminase activity of H66R mutant was approximately a half

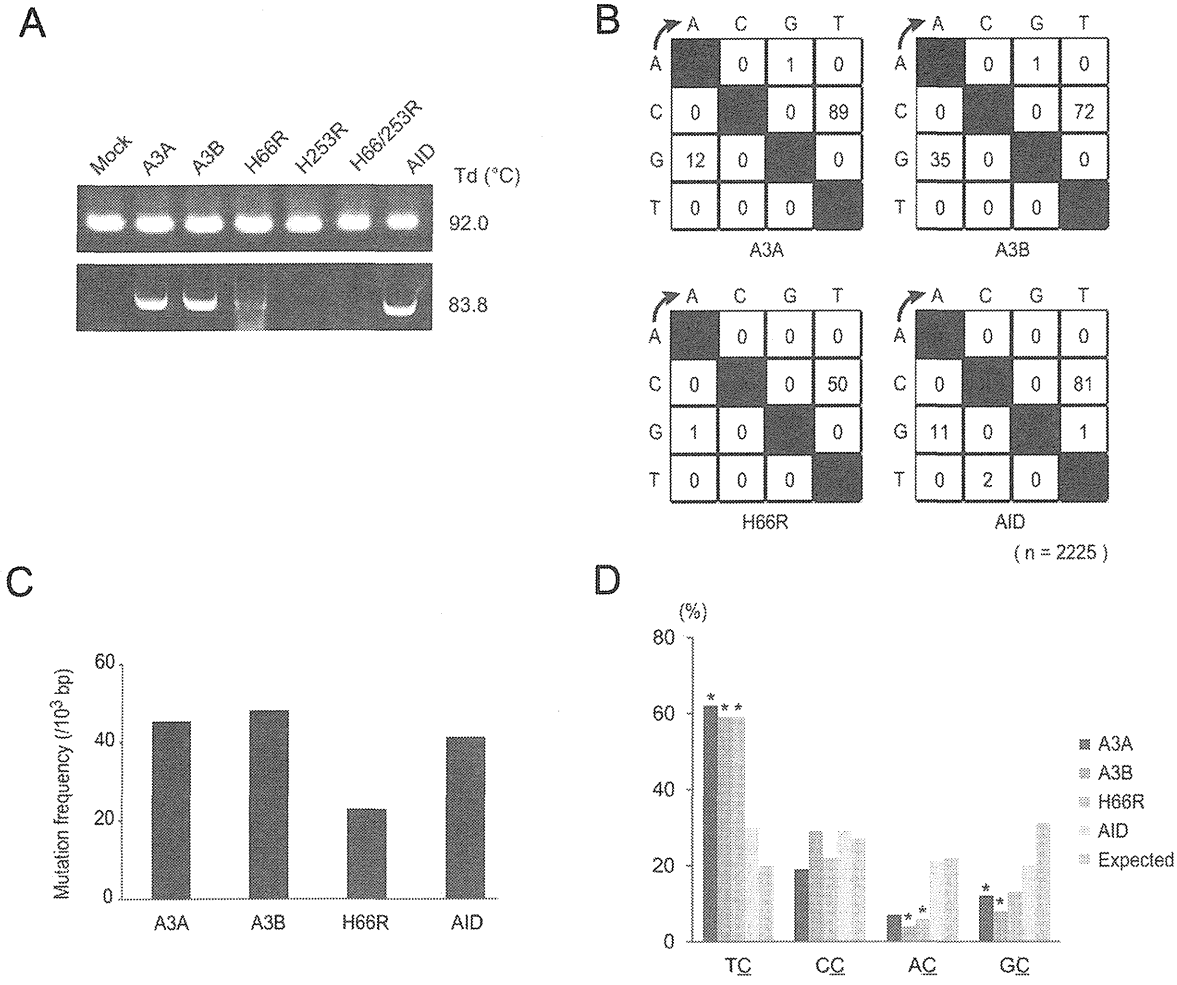

Figure 2 | Foreign DNA editing by A3A, A3B, and AID. (A) Agarose gel analyses of 3D-PCR products from HEK293 cells. Cells were transfected with expression vector for A3A, A3B wild-type or mutant, or AID together with pEGFP-N3 and pEF-UGI. Total DNA was recovered 2 days after transfection, and *EGFP* gene was amplified by 3D-PCR at the indicated denaturation temperatures (Td). (B) Mutation matrices of hyperedited *EGFP* sequences derived from cloned amplicons at 83.8°C of Td. "n" indicates the number of bases sequenced. We sequenced 5 clones (2,225 base pairs in total) in each group. (C) Frequencies of C/G to T/A transitions in hyperedited *EGFP* genes. C/G to T/A transitions per 1,000 sequenced base pairs are shown. (D) Dinucleotide contexts in foreign DNA editing. The rates of indicated dinucleotide sequence at the C to T transitions are shown. Asterisks indicate statistical significance in a χ^2 test ($p < 0.01$).

compared to that of A3B WT as seen in foreign DNA assays. The contexts of C/G to T/A transitions detected from the lowest Td amplicons in genomic DNA editing in A3-expressing cells were distinct from those in foreign DNA editing (Fig 3e). A preference for 5′-TC dinucleotide was not apparently observed, alternatively, 5′-GC dinucleotides were preferred in all samples. However, this bias fails to reach statistical significance ($p < 0.01$) in a χ^2 test. The preferred target sequences of AID editing were 5′-GC and 5′-AC dinucleotides as described by many prior studies[27,30]. Mutation frequencies and preferred target sequence of A3B was also analyzed by using amplicons at 94.0°C of Td. Mutation frequency of A3B-expressing cells were about 3 times higher than that of mock-transfected cells (Supplementary Fig. S2 online). A preference for 5′-TC dinucleotide was impaired, compared to that in foreign DNA editing assays (Supplementary Fig. S2 online). Our results reveal that in addition to AID, A3A and A3B can induce C/G to T/A transitions into human nuclear DNA without repressing proofreading enzymes (e.g., UNG). Mutation frequencies were 6 to 9 per 1000 base pairs in A3A-, A3B WT-, and AID-expressing cells, and much less frequent compared to those in foreign DNA editing. As seen with foreign DNA editing, carboxyl-terminal CDA is mainly responsible for catalytic activity but not sufficient for full editing activity. The preference context of genomic DNA editing by A3A and A3B is different from that of viral or foreign DNA editing.

Deep sequencing reveals hyperediting of human genomic DNA by A3 proteins. Amplicon sequencing by next-generation sequencer has enabled to detect extremely low levels of mutations of targeted regions in genomic DNA. To verify more certainly that A3 proteins edit human nuclear DNA, we performed deep sequencing of A3-expressing cells. HEK293/EGFP cells were transfected with an empty vector or expression vectors for A3A, A3B WT, H66/253R, or AID by lipofection, and total DNA were extracted after 7-day culture. We amplified a portion of *EGFP* gene with 443 base pair length (from thymine 56 to cytosine 498) by conventional PCR protocol, not by 3D-PCR, and performed amplicon sequencing with the coverage of 1337 to 2654 reads per sample. This analysis revealed that extremely large numbers of nucleotides were substituted over the full length of amplicons in A3A-, A3B WT-, and AID-expressing cells, whereas very few mutations were detected in mock and H66/253R-expressing cells (Supplementary Table 1 online). C/G to T/A transitions were observed most frequently in A3A-expressing cells as variation rates reach approximately 7% at the maximum, while below 3% at most in A3B- and AID-expressing cells (Fig 4a

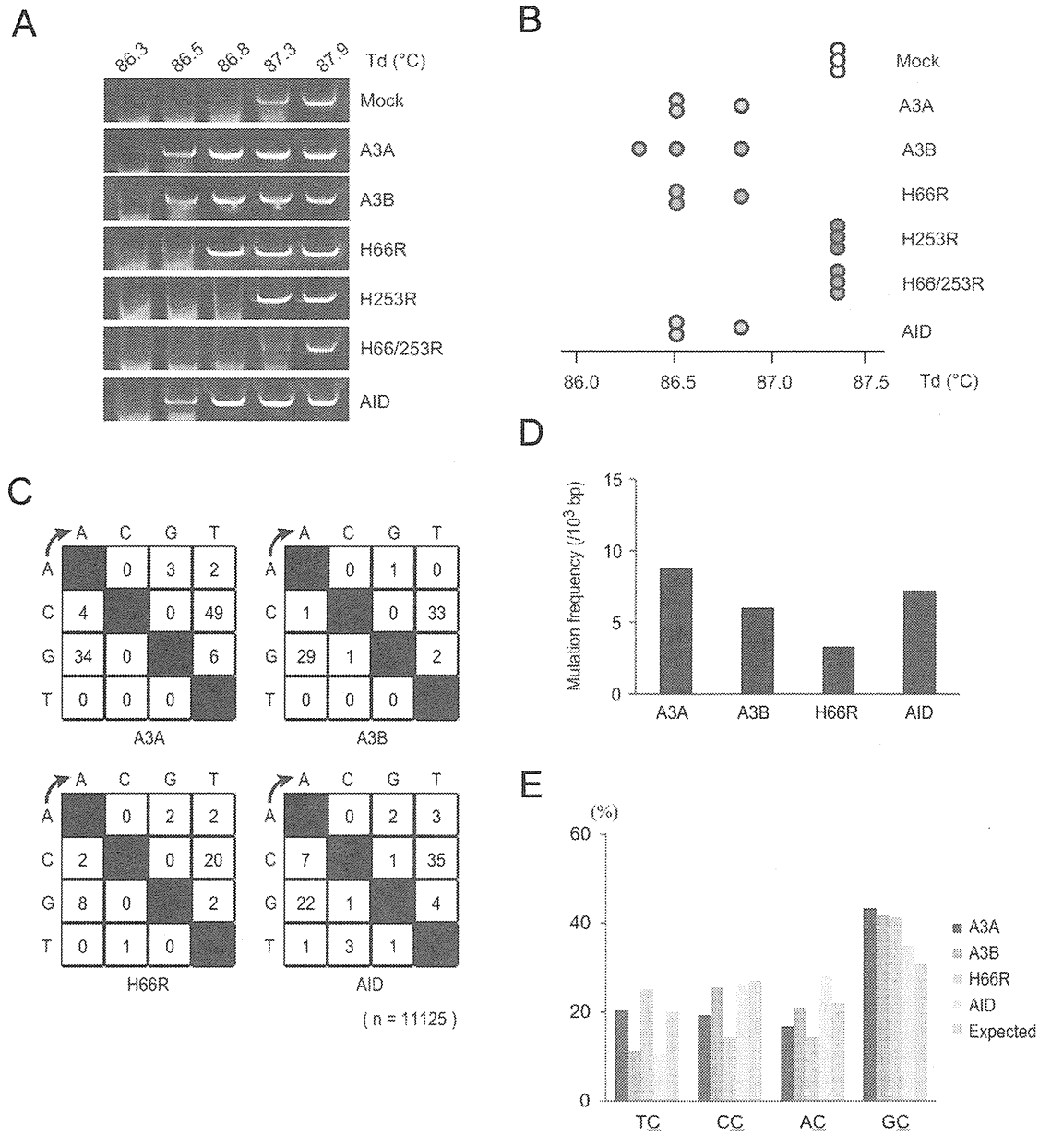

Figure 3 | Hypermutations in *EGFP* genes integrated in genomic DNA of HEK293 cells. (A) Agarose gel analyses of 3D-PCR products of *EGFP* genes extracted from HEK293/EGFP cells. Cells were transfected with expression vector for A3A, A3B wild-type or mutant, or AID. Total DNA was recovered 7 days after transfection and *EGFP* genes were amplified by 3D-PCR at the indicated denaturation temperatures (Td). (B) Distributions of the lowest denaturation temperatures for positive PCR amplification in each sample. Each circle represents independent experiment consisting of transfection, DNA extraction, and 3D-PCR. (C) Mutation matrices of hyperedited *EGFP* sequences derived from cloned PCR products at Td lower than 87°C. "n" indicates the number of bases sequenced. We sequenced 25 clones (11,125 base pairs in total) in each group. (D) Frequencies of C/G to T/A transitions in hyperedited *EGFP* genes. C/G to T/A transitions per 1,000 sequenced base pairs are shown. (E) Dinucleotide contexts in genomic DNA editing. The rates of indicated dinucleotide sequence at the C to T transitions are shown. Deviations in the editing contexts do not reach statistical significance ($p < 0.01$) in a χ^2 test.

and Supplementary Table 1 online). The mutation frequency analysis revealed that large numbers of C/G to T/A substitutions were induced in A3A-, A3B-, and AID-expressing cells, whereas other types of base substitutions were very few (Fig 4b). These results are similar to the data obtained by 3D-PCR and clonal sequencing of A3- and AID-expressing cells, and further demonstrated that A3A and A3B as well as AID can induce C/G to T/A transitions into genomic DNA in human cells with intact DNA repair systems. Dinucleotide preference of target sequence for deamination by A3A, A3B and AID was also analyzed, however, we did not found any preference in this experiment (Fig. 4C), suggesting the difference between foreign DNA editing and genomic DNA editing.

Expression of A3B and somatic mutations in lymphoma cells. Although AID has been reported to play important roles in lymphomagenesis by inducing mutations in both Ig and non-Ig genes[11,12,31–34], AID-independent mechanisms are also suggested, because AID is not expressed in all types of B-cell lymphomas[31,35]. We hypothesized that A3 may contribute to somatic mutations in some lymphoma cells. To examine this hypothesis, we first determined expression levels of *A3A*, *A3B*, and *AID* by quantitative RT-PCR in several B-cell lymphoma cell lines using peripheral blood lymphocytes (PBL) as control (Fig 5a). Our analysis revealed that *A3B* was highly expressed in 3 of 4 cell lines, particularly, markedly high in KIS1 cells, whereas expression of *A3A* transcripts was not detected in any

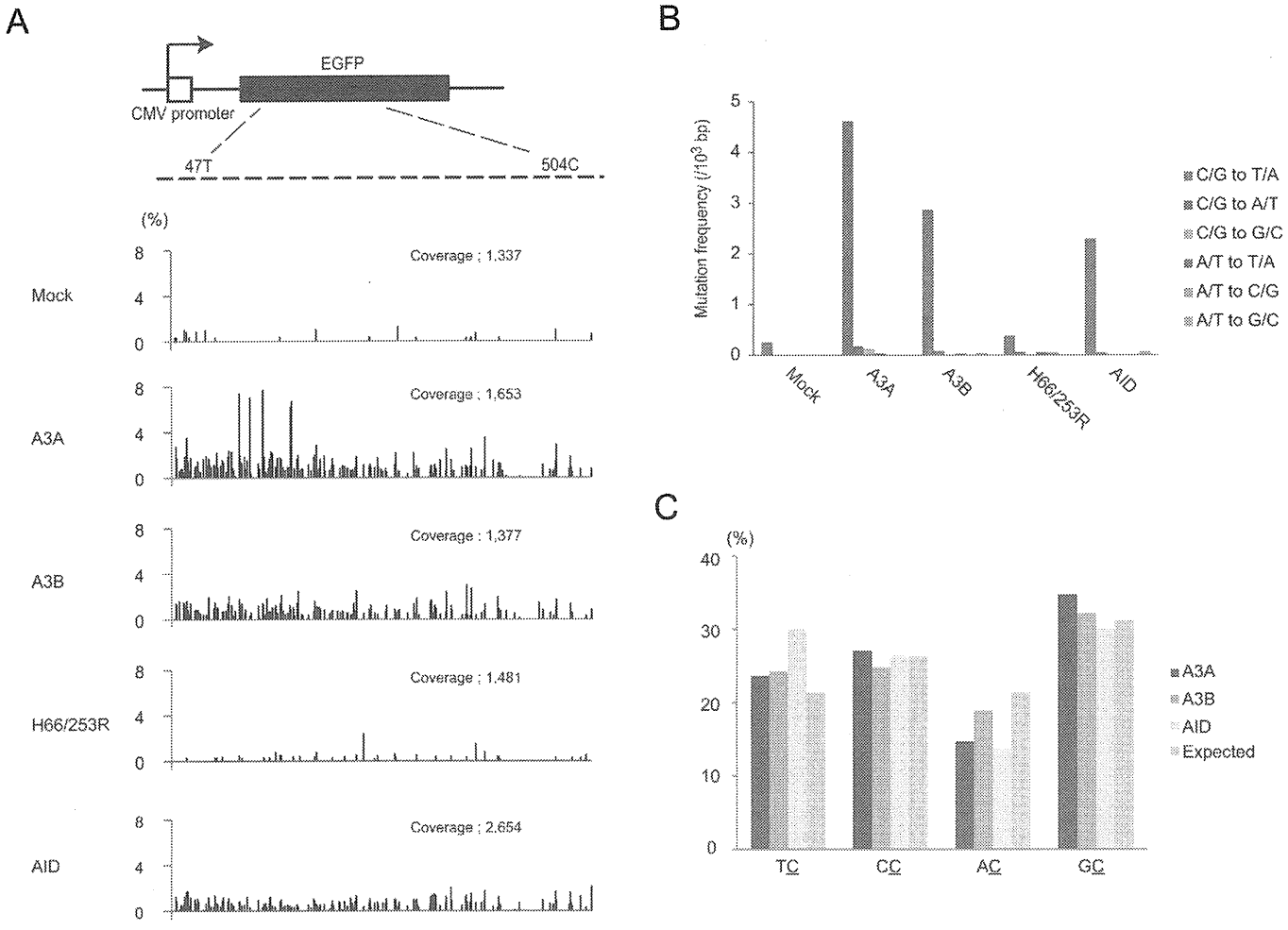

Figure 4 | Deep sequencing of *EGFP* genes in genomic DNA. (A) The distributions of C/G to T/A substitutions in the *EGFP* sequences. Total DNA was recovered form HEK293/EGFP cells 7 days after transfection with expression vector for A3A, A3B wild type or H66/253R or AID. We amplified a portion of *EGFP* sequence from thymine 47 to cytidine 504 (top schematic) by PCR with high-fidelity polymerase and sequenced the amplicons by GS-junior bench top system (Roche). Sequence data were analyzed with equipped software. "Coverage" indicates the total numbers of sequenced reads. (B) Frequencies of base substitutions in hyperedited *EGFP* genes. Base substitutions were classified to 6 groups and substituted base number of each group per 1,000 sequenced base pairs are show. (C) Dinucleotide contexts in genomic DNA editing. The rates of indicated dinucleotide sequence at the C to T transitions are shown. Deviations in the editing contexts do not reach statistical significance ($p < 0.01$) in a χ^2 test.

lymphoma cell lines consistent with prior work suggesting myeloid specificity[25,36]. *AID* transcripts were detected in 2 of 4 cell lines, which is consistent with previous studies[31,32,37]. We also examined expression of *A3B* in two lymph node samples of diffuse large B-cell lymphoma, and found that A3B is actually expressed (supplementary Fig. 3 online).

To investigate the correlation between *A3B* expression and frequency of somatic mutations, we next performed direct sequencing of *cMYC*, *PAX5*, and *A20* genes which are exemplary genes mutated frequently in B-cell lymphoma[33,38]. We compared mutation frequencies of these genes in SUDHL-6 and KIS-1, because the expression of *A3B* was the lowest in the former and the highest in the latter, while AID was not expressed in either cell line. DNA sequences between exon 1 and intron 1 of these three genes were analyzed (899 base pairs of *cMYC*, 1550 base pairs of *Pax5*, and 1088 base pairs of *A20*), since it have been reported that somatic mutations induced by cytidine deaminases were concentrated within 2 kb downstream from transcription initiation sites[33,34]. We found nine mutations within investigated sequences of *cMYC* and *PAX5* in KIS-1, but not in SUDHL-6, in which five of nine mutations detected were C/G to T/A transitions. On the other hand, no mutation was detected within sequenced region of *A20* in either cells (Fig 5b). To analyze ongoing mutations in the genome in individual cells, we next sequenced the same region of *cMYC* sub-cloned from KIS-1 and SUDHL-6, and found several more C to T mutations in KIS-1 cells, but not in SUDHL-6 cells (Supplementary Fig. S4 online). We next determined expression of these tumor-related genes by quantitative RT-PCR and found that the transcripts of *cMYC* and *PAX5* were highly expressed in both SUDHL6 and KIS1 cells as compared to PBL, whereas *A20* was less transcribed in these lymphoma cells. These results suggest that high expression of *A3B* resulted in accumulation of base alterations, especially C/G to T/A transitions, in actively transcribed tumor-related genes in lymphoma cells.

To ascertain more definitely that A3B can edit tumor-related genes in lymphoma cells, we introduced *A3B* into a lymphoma cell line and analyzed somatic mutations in *cMYC*. SUDHL-6 cells were transfected with expression vector for A3B WT, H66/253R, or mock by electroporation and total DNA was extracted after 7-day culture. With 3D-PCR analysis of *cMYC*, we obtained the amplicon from only A3B WT-expressing cells at the lower Td (Fig 6a). Clonal sequencing of amplicons at 85.9°C revealed 2 to 7 nucleotide substitutions per strand, and more than 80% of these mutations were C/G to T/A transitions, with a preference for 5′-G<u>C</u> dinucleotide sites (Fig 6b and c). We also sequenced the amplicons at 94.0°C of Td and

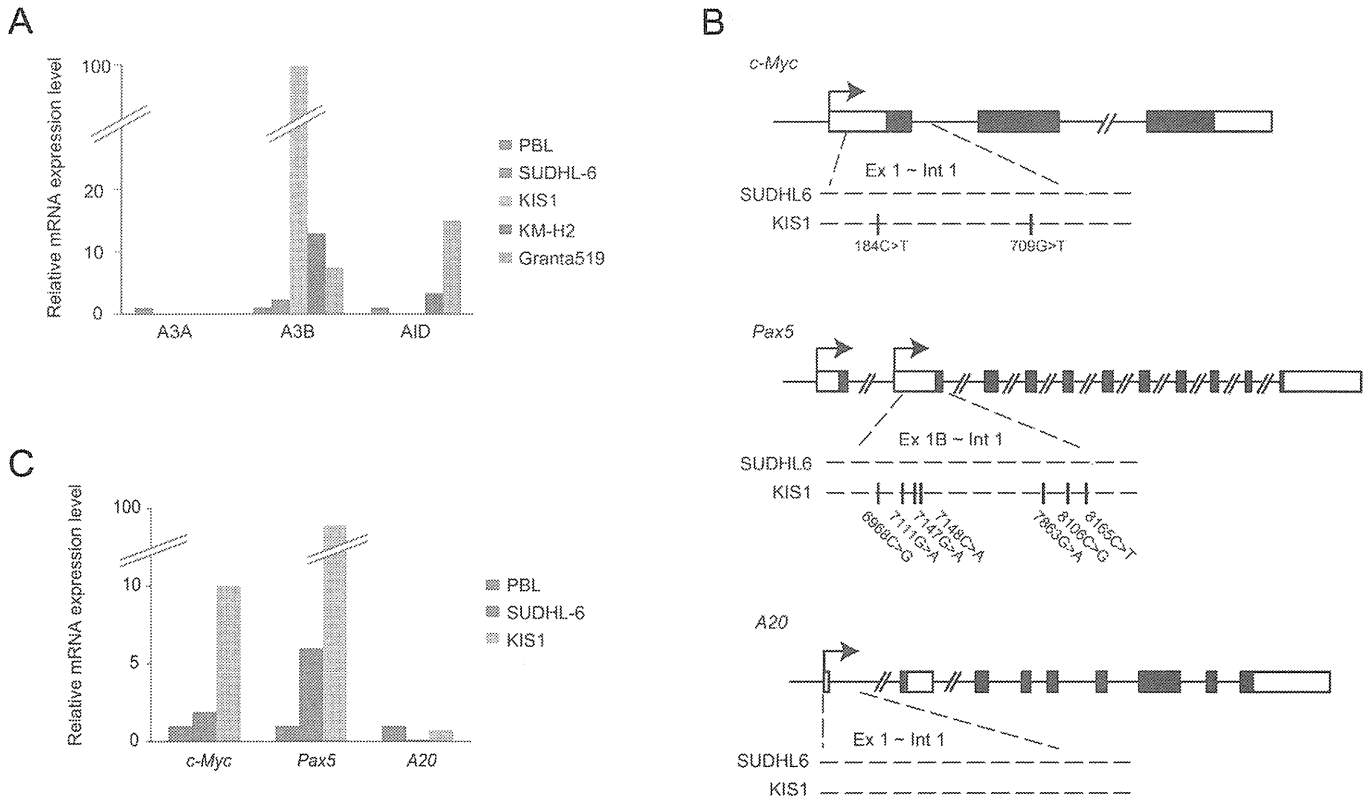

Figure 5 | Expression of *A3B* and somatic mutations in oncogenes in human lymphoma cell lines. (A) Quantitative RT-PCR for *A3A*, *A3B*, and *AID* in lymphoma cell lines. The levels of target cDNA were normalized to the endogenous hypoxanthine phosphoribosyl transferase 1 (*HPRT1*) and then compared to those in peripheral blood lymphocytes. (B) Mutational analyses of *C-myc*, *Pax5*, and *A20* in SUDH6 and KIS1 cells. We recovered total DNA from the cells and amplified the sequence between exon1 and intron1 of *C-myc*, *Pax5* and *A20* by PCR and performed direct sequencing of the amplicons. Locations of somatic mutations are shown below the loci with their positions. (C) The expression levels of transcripts of *C-myc*, *Pax5*, and *A20* in KIS1 and SUDHL6 cells. Quantitative RT-PCR was similarly performed with (a).

found A3B-induced C/G to T/A transitions without 5′-TC dinucleotide preference (supplementary Fig. 5 online). These data demonstrate that expression of A3B can induce somatic mutations into actively transcribed tumor-related genes in lymphoma cells.

Discussion

To date, most studies on A3 proteins have focused on their abilities as antiviral or antitransposon factors, whereas the capability of A3 proteins to induce mutations into genomic DNA in host cells has been scarcely verified. In contrast, many studies have elucidated that AID induces somatic mutations into not only Ig genes, but also tumor-related genes in human cells and that ubiquitous expression of AID in mice leads to cancers of various organs as well as lymphomas, with the accumulation of nucleotides alterations[9–13]. Thus, AID has been considered as the only DNA cytosine deaminase that can induce somatic mutations into human genome and has potential to cause cancers or hematologic malignancies.

Suspène *et al.* have recently reported that hyperediting of both mitochondrial and nuclear DNA was detected in human cells defective for UNG derived from hyper IgM syndrome patients and demonstrated that A3A-induced mutations in nuclear DNA are detectable under the condition of suppressing UNG in human cells[19]. In their report, deamination of nuclear DNA was not observed in cells expressing other A3 proteins or in cells expressing A3A without UNG suppression. Furthermore, Landry *et al.* have reported that expression of A3A together with UGI in mammalian cell lines resulted in breaking of DNA and activation of DNA damage response in a deaminase-dependent manner[18]. In these two reports, the effect on genomic integrity by A3A was dependent on the presence of UGI. Thus, there has been no direct evidence that A3 proteins induce mutations in genomic DNA in the cells with intact DNA repair systems.

In this study, we demonstrate that A3A and A3B as well as AID can induce C/G to T/A transitions into nuclear DNA without suppressing UNG by two different assays, 3D-PCR and deep sequencing. We assume that increased number of cytidine deamination catalyzed by highly expressed A3A or A3B exceeded the processivity of DNA repair enzymes such as UNG and resulted in leaving C/G to T/A transitions in nuclear DNA. Mutation frequencies were considerably lower compared to Suspène's report. However, Yoshikawa *et al.* reported that AID induced hypermutations into an actively transcribed gene in fibroblasts and that the mutation frequency was approximately 4 to 6 per 1000 base pairs[10], almost to the same extent as our results. Hence the frequency of mutations induced by cytidine deaminases into nuclear DNA is probably this extent or less in the cells with intact DNA repair systems.

We also find that *A3B* is highly expressed in several lymphoma cell lines and that the cells expressing high levels of *A3B* actually possesses somatic mutations, especially C/G to T/A transitions, in actively transcribed tumor-related genes. Furthermore, we reveal that introduction of *A3B* into lymphoma cells induces the accumulation of C/G to T/A transitions in *cMYC* gene. This is the first report that suggests the involvement of A3B in inducing somatic mutations of oncogenes in tumor cells. Together with the microarray database of A3B expression in miscellaneous cancer cell lines[14] (NextBio: http://www.nextbio.com), it is possible that A3B may induce somatic mutations into tumor related genes in various types of cancers.

Several questions remain open. First, it remains unclear what is preferred target sequences of A3 proteins in genomic DNA. Because

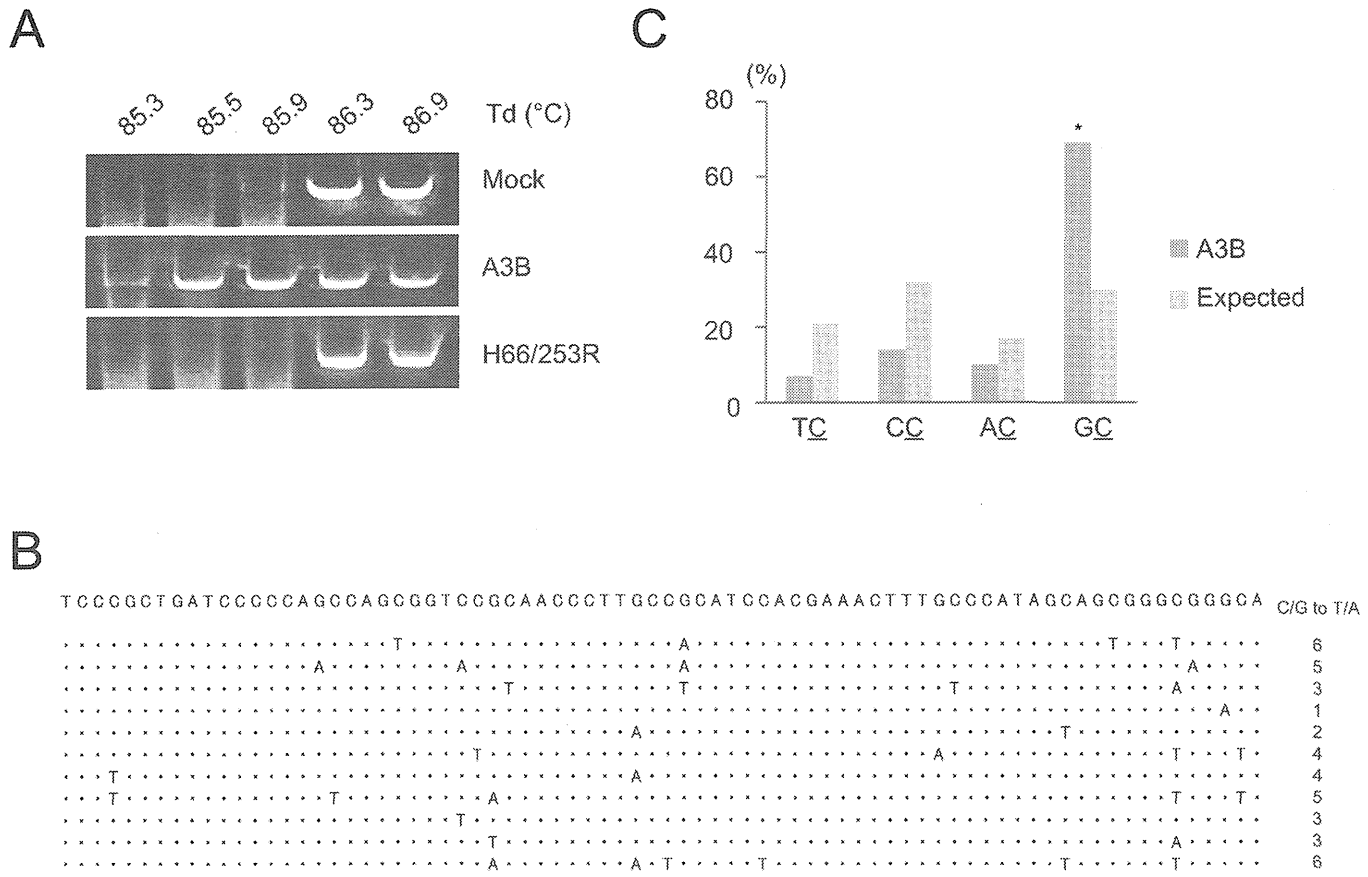

Figure 6 | A3B induced somatic mutations into *c-myc* gene in human lymphoma cells. (A) Agarose gel analyses of 3D-PCR products of *c-Myc* genes in SUDHL6. We transfected expression vector for A3B wild-type or H66/253R or empty vector and recovered total DNA 7 days after transfection. *C-myc* genes were amplified by 3D-PCR at the indicated denaturation temperatures (Td). (B) Clonal sequencing of amplicons from A3B-WT expressing SUDHL6 cells. We sequenced 11 clones (5104 base pairs in total). Seventy six bases from thymine 310 to adenine 385 in which mutations are concentrated among sequenced 464 base pairs are shown. The numbers of C/G to T/A substitutions in sequenced 464 base pair length are shown at the right end. (C) Dinucleotide contexts of somatic mutations in *c-Myc* gene by A3B. The rates of indicated dinucleotide sequence at the C to T transitions are shown. Asterisks indicate statistical significance in a χ^2 test ($p < 0.01$).

in several cancers such as breast cancer and melanoma, 5′-TC is the most prevalent target in C to T base substitutions, A3 is the most potential candidate to induce these mutations[25,28]. However, in our results, neither A3A nor A3B had a definite preference of editing site in nuclear DNA editing, whereas a preference for 5′-TC dinucleotide was observed in foreign DNA editing as previously reported. It is possible that A3A and A3B have no distinct favorite context in nuclear DNA editing, unlike viral and bacterial DNA editing, because human genomic DNA is more profoundly protected in transcription than viral or bacterial DNA and is under survey of DNA repair systems. However, Suspene *et al.* reported that target contexts of cytidine deamination in A3A+UGI-expressing cells were 5′-TC and 5′-CC dinucleotides, which were identical to the contexts of viral or bacterial DNA editing[19]. We assume that this discrepancy might be attributable to cell types or expression levels in cells. Hence, further analyses should be required to clarify the favorite target contexts of A3 proteins in nuclear DNA editing. The second question is how transcriptional control and post-translational modification of A3 proteins regulate A3 activity. Because the molecules that possess a capability of editing nuclear DNA threaten cell homeostasis, expression and activity of A3A and A3B must be strictly controlled. AID is known to be regulated at multiple steps[39], for example, transcriptional regulation[40–42], post-transcriptional regulation by micro-RNA[43,44], regulation of intracellular localization[45,46], and phosphorylation by PKA[47,48]. In contrast to AID, little is known about how A3 proteins are regulated. It has been reported that A3A is abundantly expressed in CD14+ monocytes and upregulated by interferon-α stimulation[25,49,50]. Meanwhile, it is not clear where A3B is expressed normally[25,42,49,50] and how it is regulated. As for post-translational modification, we previously reported that PKA-mediated phosphorylation of A3G regulates the interaction between A3G and HIV Vif[51]. To better understand the physiological roles of A3 proteins, it is important to elucidate how their expression and activity are regulated. The last question is whether A3 proteins can serve as an "initiator" of tumorigenesis. Our results suggest A3B indeed induces somatic mutations into genomic DNA in various human tumor cells, however, it is unclear whether A3B proteins impair genomic DNA from the early stage of oncogenesis. To address this question, hereafter, histopathological and genetic analyses of transgenic mouse constitutively expressing A3 proteins are necessary.

In conclusion, our findings provides the first evidence that A3A and A3B can induce C/G to T/G transitions into genomic DNA without suppressing DNA repair system. Our data also show that high expression of *A3B* is related to mutation frequencies of oncogenes in lymphoma cells. Our results suggest that *A3B* is an oncogene, like AID, which may have the capacity to evoke genomic instability through base substitutions in human cells. Further studies will be required to test whether endogenous A3B is capable of impairing genomic integrity as a DNA mutator and contributing to the development of human cancers and hematologic malignancies.

Methods

DNA constructs and cell lines. Plasmids containing coding sequence of human *A3A* and *A3B* were kindly provided by Dr. Kenzo Tokunaga[21]. Expression vectors for HA-tagged A3A, A3B and AID were generated by sub-cloning of coding sequences into pCAG-GS vector. A3B catalytic domain mutants (H66R, H253R, and H66/253R) were generated by KOD-plus mutagenesis Kit (Toyobo). Expression vector for Uracil-DNA glycosylase inhibitor, pEF-UGI was kindly provided by Dr. Ruben S Harris[25]. HEK293 and HEK293T cells were maintained with Dulbecco's modified Eagle's medium containing 10% of fetal bovine serum (FBS) and penicillin, streptomycin, and glutamine (PSG). All B-cell lymphoma cell lines were maintained with RPMI1640 containing 10% FBS and PSG. Retrovirus containing *EGFP* sequence was produced by co-transfection of pMLV gag-pol, VSV-G, and pDON-EGFP into HEK293T cells. HEK293/EGFP cells were generated by retroviral transduction of *EGFP* and selection of 1 mg/ml G418 for two months.

Immunoblotting. HEK293 cells were transfected with expression vector for A3A, A3B wild-type or mutant (H66R, H253R or H66/253R) or AID, and lysed with RIPA buffer (50 mM Tris-HCl pH7.5, 150 mM NaCl, 1 mM EDTA, 1% Triton-X, 0.1% SDS, 0.1% DOC) after 2-day culture. After centrifugation at 20,000 x g for 15 min, supernatant was mixed with sample buffer (Biorad), boiled for 5 minutes, resolved on 12% (w/v) polyacrylamide gel, transferred to PVDF membrane (Immobilon, Millipore), and analyzed by standard immunoblotting procedure with anti-HA monoclonal antibody (12CA5, Roche) or anti-β-actin monoclonal antibody (AC-15, Sigma).

3D-PCR and clonal sequencing. For foreign DNA editing assay, HEK293 cells were transfected with pEGFP-N3, pEF-UGI, and expression vector for A3A, A3B WT or mutant, or AID by using Fugene HD (Roche). After two-day culture, total DNA was extracted by using Quick Gene DNA whole blood kit (Fuji Film). First round PCR was performed with primers listed in Supplementary Table S2 using rTaq DNA polymerase (Takara), with the following reaction profile; 30 s at 94°C, 25cycles of 30 s at 94°C, 40 s at 62°C, and 90 s at 72°C followed by 10 min at 72°C. The amplicons were separated by electrophoresis on 1% (w/v) agarose gel, and extracted from the gel using Qiaquick Gel Extraction kit (Qiagen). We used 25 ng of first-round PCR products as template for nested PCR using Hotstar Hifidelity DNA polymerase (Qiagen), with the following reaction profile; 5 min at 95°C, 35 cycles of 15 s at 83–92°C, 60 s at 62°C, 80 s at 72°C, followed by 10 min at 72°C. The amplicons derived at 83.8°C were cloned into pT7-blue vector (Novagen). For nuclear DNA editing assay, HEK293/EGFP cells were transfected with expression vector for A3A, A3B WT or mutants, or AID using Fugene HD (Roche). Seven days after transfection, we extracted total DNA from these cells with the same method of foreign DNA editing assay. First round PCR was performed using Advantage HF2 polymerase kit (Clontech), with the following reaction profile;1 min at 94°C, 30 cycles of 30 s at 94°C followed by 2 min at 68°C, followed by 3 min at 68°C. We used 25 ng of first-round PCR products for nested PCR using Hotstar Hifidelity DNA polymerase (Qiagen) with the following reaction profile; 5 min at 95°C, 35 cycles of 15 s at 86–89°C, 60 s at 62°C, and 80 s at 72°C, followed by 10 min at 72°C. The amplicons derived at 86.5°C and 83.8°C were cloned into pT7-blue vector (Novagen). For *c-myc* gene editing assay in lymphoma cells, we transfected SUDHL6 cells with expression vectors for A3B WT or H66/253R by electroporation using Nucleofector (Amaxa) and extracted total DNA from the cells 7 days after transfection. First round PCR and gel extractions of amplicons were performed with the same methods of nuclear DNA editing assay. We used 25 ng of first-round PCR products for nested PCR using Hotstar Hifidelity DNA polymerase (Qiagen), with the following reaction profile; 5 min at 95°C, 35 cycles of 15 s at 85–88°C, 60 s at 62°C, 80 s at 72°C, followed by 10 min at 72°C. The amplicons derived at 85.3°C were cloned into pT7-blue vector (Novagen) and sequenced using 3130xl Genetic Analyzer (Applied Biosystems).

Deep sequencing. Total DNA was extracted from HEK293/EGFP transfected with expression vectors for A3A, A3B WT or H66/253R or AID 7 days after transfection. A portion of *EGFP* gene with 443 base pair length, from thymine 56 to cytosine 498, was amplified with the primers listed in Supplementary Table 2 using Advantage HF2 polymerase kit (Clontech), with the following reaction profile; 1 min at 94°C, 30 cycles of 30 s at 94°C followed by 2 min at 68°C, and followed by 3 min at 68°C. The amplicons were separated by electrophoresis on 1% (w/v) agarose gel, and extracted from the gel using Quiaquick Gel Extraction Kit (Qiagen). Purified amplicons were sequenced using GS junior bench top system (Roche) according to the manufacturer's protocol and analyzed with equipped software, GS Amplicon Variant Analyzer.

Lymphoma cell lines and patient samples. Four B-cell lymphoma cell lines (SUDHL6, KIS1, KM-H2, and Granta519) were cultured in RPMI1640 containing 10% of fetal bovine serum (FBS) and penicillin, streptomycin, and glutamine (PSG). We extracted total DNA from these cells by using Quick Gene DNA whole blood kit (Fuji Film) and total RNA by using mir Vana miRNA isolation kit (Ambion). Tumor biopsy specimens prior to treatment were obtained from two patients with diffuse large B-cell lymphoma. The study was approved by the Kyoto University Institutional Review Board and written informed consent was obtained from each patient. Total RNA were extracted similarly to lymphoma cell lines. Naïve B-cells were isolated from healthy donor's peripheral blood by using MACS® naive B cell isolation kit (Miltenyi Biotec).

Quantitative RT-PCR. Complementary DNA was synthesized from 200 ng of total RNA using Revertra Ace qPCR RT Master Mix (Toyobo). Real-time PCR were performed with Thunderbird SYBR qPCR Mix (Toyobo) according to manufacturer's protocol. Target cDNAs were normalized to the endogenous expression level of the house keeping reference gene for hypoxanthine-guanine phosphoribosyl transferase 1 (*HPRT1*) or glyceraldehyde 3-phosphate dehydrogenase (*GAPDH*). All primers for real-time PCR are listed in Supplementary Table 2.

Sequencing of oncogenes from lymphoma cell lines. We amplified portions of *C-myc*, *Pax5*, and *A20* from with the primers listed in Supplementary Table 2 using Advantage HF2 polymerase kit (Clontech), with the following reaction profile; 1 min at 94°C, 30 cycles of 30 s at 94°C followed by 4 min at 68°C, and followed by 3 min at 68°C. The amplicons were separated by electrophoresis on 1% (w/v) agarose gel, extracted from the gel using Qiaquick Gel Extraction kit (Qiagen), and sequenced using 3130xl Genetic Analyzer (Applied Biosystems). In *c-Myc* clonal sequencing, the amplicon was subcloned into pTA2-vector (TOYOBO) and subsequently sequenced.

1. Hahn, W. C. & Weinberg, R. A. Rules for making human tumor cells. *N Engl J Med* **347**, 1593–603 (2002).
2. Pleasance, E. D. *et al.* A comprehensive catalogue of somatic mutations from a human cancer genome. *Nature* **463**, 191–6 (2010).
3. Bronner, C. E. *et al.* Mutation in the DNA mismatch repair gene homologue hMLH1 is associated with hereditary non-polyposis colon cancer. *Nature* **368**, 258–61 (1994).
4. Greenman, C. *et al.* Patterns of somatic mutation in human cancer genomes. *Nature* **446**, 153–8 (2007).
5. Prickett, T. D. *et al.* Analysis of the tyrosine kinome in melanoma reveals recurrent mutations in ERBB4. *Nat Genet* **41**, 1127–32 (2009).
6. Macduff, D. A. & Harris, R. S. Directed DNA deamination by AID/APOBEC3 in immunity. *Curr Biol* **16**, R186–9 (2006).
7. Conticello, S. G. The AID/APOBEC family of nucleic acid mutators. *Genome Biol* **9**, 229 (2008).
8. Muramatsu, M. *et al.* Class switch recombination and hypermutation require activation-induced cytidine deaminase (AID), a potential RNA editing enzyme. *Cell* **102**, 553–63 (2000).
9. Matsumoto, Y. *et al.* Helicobacter pylori infection triggers aberrant expression of activation-induced cytidine deaminase in gastric epithelium. *Nat Med* **13**, 470–6 (2007).
10. Yoshikawa, K. *et al.* AID enzyme-induced hypermutation in an actively transcribed gene in fibroblasts. *Science* **296**, 2033–6 (2002).
11. Okazaki, I. M. *et al.* Constitutive expression of AID leads to tumorigenesis. *J Exp Med* **197**, 1173–81 (2003).
12. Pasqualucci, L. *et al.* AID is required for germinal center-derived lymphomagenesis. *Nat Genet* **40**, 108–12 (2008).
13. Endo, Y. *et al.* Activation-induced cytidine deaminase links between inflammation and the development of colitis-associated colorectal cancers. *Gastroenterology* **135**, 889–98, 898 e1-3 (2008).
14. Jarmuz, A. *et al.* An anthropoid-specific locus of orphan C to U RNA-editing enzymes on chromosome 22. *Genomics* **79**, 285–96 (2002).
15. Goila-Gaur, R. & Strebel, K. HIV-1 Vif, APOBEC, and intrinsic immunity. *Retrovirology* **5**, 51 (2008).
16. Mangeat, B. *et al.* Broad antiretroviral defence by human APOBEC3G through lethal editing of nascent reverse transcripts. *Nature* **424**, 99–103 (2003).
17. Bogerd, H. P. *et al.* Cellular inhibitors of long interspersed element 1 and Alu retrotransposition. *Proc Natl Acad Sci U S A* **103**, 8780–5 (2006).
18. Landry, S., Narvaiza, I., Linfesty, D. C. & Weitzman, M. D. APOBEC3A can activate the DNA damage response and cause cell-cycle arrest. *EMBO Rep* **12**, 444–50 (2011).
19. Suspène, R. *et al.* Somatic hypermutation of human mitochondrial and nuclear DNA by APOBEC3 cytidine deaminases, a pathway for DNA catabolism. *Proc Natl Acad Sci U S A* **108**, 4858–63 (2011).
20. Lackey, L. *et al.* APOBEC3B and AID have similar nuclear import mechanisms. *J Mol Biol* **419**, 301–14 (2012).
21. Kinomoto, M. *et al.* All APOBEC3 family proteins differentially inhibit LINE-1 retrotransposition. *Nucleic Acids Res* **35**, 2955–64 (2007).
22. Bogerd, H. P., Wiegand, H. L., Doehle, B. P. & Cullen, B. R. The intrinsic antiretroviral factor APOBEC3B contains two enzymatically active cytidine deaminase domains. *Virology* **364**, 486–93 (2007).
23. Suspène, R. *et al.* Extensive editing of both hepatitis B virus DNA strands by APOBEC3 cytidine deaminases in vitro and in vivo. *Proc Natl Acad Sci U S A* **102**, 8321–6 (2005).
24. Bonvin, M. & Greeve, J. Effects of point mutations in the cytidine deaminase domains of APOBEC3B on replication and hypermutation of hepatitis B virus in vitro. *J Gen Virol* **88**, 3270–4 (2007).
25. Stenglein, M. D., Burns, M. B., Li, M., Lengyel, J. & Harris, R. S. APOBEC3 proteins mediate the clearance of foreign DNA from human cells. *Nat Struct Mol Biol* **17**, 222–9 (2010).
26. Suspène, R., Henry, M., Guillot, S., Wain-Hobson, S. & Vartanian, J. P. Recovery of APOBEC3-edited human immunodeficiency virus G->A hypermutants by differential DNA denaturation PCR. *J Gen Virol* **86**, 125–9 (2005).

27. Vartanian, J. P. *et al.* Massive APOBEC3 editing of hepatitis B viral DNA in cirrhosis. *PLoS Pathog* **6**, e1000928 (2010).
28. Bishop, K. N. *et al.* Cytidine deamination of retroviral DNA by diverse APOBEC proteins. *Curr Biol* **14**, 1392–6 (2004).
29. Harris, R. S. *et al.* DNA deamination mediates innate immunity to retroviral infection. *Cell* **113**, 803–9 (2003).
30. Beale, R. C. *et al.* Comparison of the differential context-dependence of DNA deamination by APOBEC enzymes: correlation with mutation spectra in vivo. *J Mol Biol* **337**, 585–96 (2004).
31. Greeve, J. *et al.* Expression of activation-induced cytidine deaminase in human B-cell non-Hodgkin lymphomas. *Blood* **101**, 3574–80 (2003).
32. Deutsch, A. J. *et al.* MALT lymphoma and extranodal diffuse large B-cell lymphoma are targeted by aberrant somatic hypermutation. *Blood* **109**, 3500–4 (2007).
33. Pasqualucci, L. *et al.* Hypermutation of multiple proto-oncogenes in B-cell diffuse large-cell lymphomas. *Nature* **412**, 341–6 (2001).
34. Kotani, A. *et al.* A target selection of somatic hypermutations is regulated similarly between T and B cells upon activation-induced cytidine deaminase expression. *Proc Natl Acad Sci U S A* **102**, 4506–11 (2005).
35. Smit, L. A. *et al.* Expression of activation-induced cytidine deaminase is confined to B-cell non-Hodgkin's lymphomas of germinal-center phenotype. *Cancer Res* **63**, 3894–8 (2003).
36. Chen, H. *et al.* APOBEC3A is a potent inhibitor of adeno-associated virus and retrotransposons. *Curr Biol* **16**, 480–5 (2006).
37. Mottok, A., Hansmann, M. L. & Bräuninger, A. Activation induced cytidine deaminase expression in lymphocyte predominant Hodgkin lymphoma. *J Clin Pathol* **58**, 1002–4 (2005).
38. Kato, M. *et al.* Frequent inactivation of A20 in B-cell lymphomas. *Nature* **459**, 712–6 (2009).
39. Delker, R. K., Fugmann, S. D. & Papavasiliou, F. N. A coming-of-age story: activation-induced cytidine deaminase turns 10. *Nat Immunol* **10**, 1147–53 (2009).
40. Crouch, E. E. *et al.* Regulation of AID expression in the immune response. *J Exp Med* **204**, 1145–56 (2007).
41. Gonda, H. *et al.* The balance between Pax5 and Id2 activities is the key to AID gene expression. *J Exp Med* **198**, 1427–37 (2003).
42. Pauklin, S., Sernández, I. V., Bachmann, G., Ramiro, A. R. & Petersen-Mahrt, S. K. Estrogen directly activates AID transcription and function. *J Exp Med* **206**, 99–111 (2009).
43. Teng, G. *et al.* MicroRNA-155 is a negative regulator of activation-induced cytidine deaminase. *Immunity* **28**, 621–9 (2008).
44. de Yébenes, V. G. *et al.* miR-181b negatively regulates activation-induced cytidine deaminase in B cells. *J Exp Med* **205**, 2199–206 (2008).
45. Ito, S. *et al.* Activation-induced cytidine deaminase shuttles between nucleus and cytoplasm like apolipoprotein B mRNA editing catalytic polypeptide 1. *Proc Natl Acad Sci U S A* **101**, 1975–80 (2004).
46. Patenaude, A. M. *et al.* Active nuclear import and cytoplasmic retention of activation-induced deaminase. *Nat Struct Mol Biol* **16**, 517–27 (2009).
47. Basu, U. *et al.* The AID antibody diversification enzyme is regulated by protein kinase A phosphorylation. *Nature* **438**, 508–11 (2005).
48. McBride, K. M. *et al.* Regulation of class switch recombination and somatic mutation by AID phosphorylation. *J Exp Med* **205**, 2585–94 (2008).
49. Koning, F. A. *et al.* Defining APOBEC3 expression patterns in human tissues and hematopoietic cell subsets. *J Virol* **83**, 9474–85 (2009).
50. Berger, G. *et al.* APOBEC3A is a specific inhibitor of the early phases of HIV-1 infection in myeloid cells. *PLoS Pathog* **7**, e1002221 (2011).
51. Shirakawa, K. *et al.* Phosphorylation of APOBEC3G by protein kinase A regulates its interaction with HIV-1 Vif. *Nat Struct Mol Biol* **15**, 1184–91 (2008).

Acknowledgments

We thank R. Harris for thoughtful feedback and for UGI vector, and K. Tokunaga for A3A and A3B vectors.

Author contributions

M.S. performed most of the experiments, analyzed the data and wrote the manuscript; I.K., M.M., T.S. and K.T. performed sequencing of lymphoma cell lines; K.S. and N.K. wrote the manuscript; M.K. established q-PCR; A.T.K. designed the experiments and wrote the manuscript.

Additional information

Supplementary information accompanies this paper at http://www.nature.com/scientificreports

Competing interest statements: The authors declare no competing financial interests.

How to cite this article: Shinohara, M. *et al.* APOBEC3B can impair genomic stability by inducing base substitutions in genomic DNA in human cells. *Sci. Rep.* **2**, 806; DOI:10.1038/srep00806 (2012).

European Journal of Immunology

The tyrosine kinase inhibitor dasatinib suppresses cytokine production by plasmacytoid dendritic cells by targeting endosomal transport of CpG DNA

Haruyuki Fujita[1], Toshio Kitawaki[1], Takayuki Sato[1], Takahiro Maeda[2], Shimeru Kamihira[3], Akifumi Takaori-Kondo[1] and Norimitsu Kadowaki[1,4]

[1] Department of Hematology and Oncology, Graduate School of Medicine, Kyoto University, Kyoto, Japan
[2] Department of Island and Community Medicine, Nagasaki University Graduate School of Biomedical Sciences, Nagasaki, Japan
[3] Department of Laboratory Medicine, Nagasaki University Graduate School of Biomedical Sciences, Nagasaki, Japan
[4] Japan Science and Technology Agency, Core Research for Evolutional Science and Technology (CREST), Tokyo, Japan

Plasmacytoid dendritic cells (pDCs) produce a vast amount of interferon (IFN)-α in response to nucleic acids from viruses and damaged self-cells through Toll-like receptor (TLR)7 and TLR9. Pharmaceutical agents that suppress IFN-α production by pDCs are instrumental in elucidating the mechanisms behind IFN-α production, and in developing novel therapies for inflammatory disorders that involve pDCs. Here, we show that a tyrosine kinase inhibitor for chronic myeloid leukemia with multiple targets, dasatinib, strongly suppresses production of IFN-α and proinflammatory cytokines by human pDCs stimulated with multimeric CpG oligodeoxynucleotides (CpG-A) without reducing viability. In contrast, other tyrosine kinase inhibitors, imatinib, and nilotinib, did not suppress the cytokine production at clinically relevant concentrations. Inhibitors of SRC family kinases (SFKs), which are prominent targets of dasatinib, also suppressed the cytokine production. Notably, however, dasatinib, but not SFK inhibitors, abrogated prolonged localization of CpG-A in early endosomes, which is a critical step for pDCs to produce a large amount of IFN-α. This study suggests that dasatinib suppresses IFN-α production by pDCs by inhibiting SFK-dependent pathways and SFK-independent endosomal retention of CpG DNA. Kinases controlling the distinctive endosomal trafficking in pDCs may be exploited as targets to develop novel therapies for pDC-related inflammatory disorders.

Keywords: Dasatinib · Interferon · Plasmacytoid dendritic cells (pDCs) · TLR9

Additional supporting information may be found in the online version of this article at the publisher's web-site

Introduction

Plasmacytoid DCs (pDCs) are a distinctive immune cell type that produces a vast amount of IFN-α in response to virus-derived CpG DNA or ssRNA through TLR9 or TLR7, respectively [1], thus

Correspondence: Dr. Norimitsu Kadowaki
e-mail: kadowaki@kuhp.kyoto-u.ac.jp

playing an important role in antiviral immunity. pDCs also produces IFN-α in response to nucleic acids derived from damaged self-tissues, and are thereby implicated in provoking inflammatory disorders such as lupus and psoriasis [2,3]. Thus, pharmaceutical agents that suppress IFN-α production by pDCs are instrumental in elucidating mechanisms of the production of a large amount of IFN-α and in developing novel therapies for inflammatory disorders that involve pDCs.

A variety of protein kinases is involved in signaling pathways in immune responses. Antitumor kinase inhibitors that have different targets may be useful to dissect such pathways. Three tyrosine kinase inhibitors (TKIs), imatinib, nilotinib, and dasatinib, have been approved for the treatment of chronic myeloid leukemia (CML) and Philadelphia $(Ph)^+$ acute lymphoblastic leukemia (ALL), which are caused by constitutive activation of an ABL tyrosine kinase [4]. Notably, dasatinib is capable of inhibiting a broad array of tyrosine kinases in addition to ABL, among which SRC family kinases (SFKs) are prominent targets [5]. As a consequence, it has been shown that dasatinib inhibits activation of T cells [6,7] and NK cells [8,9] in vitro. However, it has not been reported whether dasatinib affects immunostimulatory activity of DCs, which play a pivotal role in the induction of innate and adaptive immune responses.

Here, we investigated the effect of dasatinib on human pDCs in comparison with the effects of the other TKIs, imatinib, and nilotinib [10]. We show that clinically relevant concentrations of dasatinib, but not imatinib or nilotinib, strongly suppressed the production of IFN-α and proinflammatory cytokines by pDCs without impairing viability. Mechanistic analysis suggests that dasatinib suppresses IFN-α production by pDCs through inhibiting both SFK-dependent pathways and SFK-independent endosomal retention of CpG DNA, which is a critical step for pDCs to produce a large amount of IFN-α [11,12]. These results have significant implications for dissecting the mechanisms of IFN-α production by pDCs and for developing novel therapies for pDC-related inflammatory disorders.

Results

Dasatinib suppresses cytokine production by pDCs stimulated with TLR9 and TLR7 ligands

There are two major types of CpG oligodeoxynucleotides (ODNs), CpG-A, and CpG-B [13]. CpG-A forms large multimeric aggregates, whereas CpG-B are monomeric and do not form such high order structure [14]. CpG-A shares its particle-like physical features with viral particles and an aggregated self-DNA-antimicrobial peptide complex observed in psoriatic lesions [15]. These particle-like nucleic acids induce pDCs to produce a large amount of IFN-α due to their prolonged retention in early endosomes [11,12]. Thus, we first examined whether dasatinib suppresses IFN-α production by pDCs stimulated with two TLR9 ligands, ODN2216 (CpG-A) or HSV-1. We also stimulated pDCs with a TLR7 ligand, influenza virus, which similarly induces a large amount of IFN-α production by pDCs. When we stimulated PBMCs depleted of pDCs with ODN2216, IFN-α was scarcely detected in the supernatant (Supporting Information Fig. 1), indicating that pDCs are virtually the only cell type among PBMCs that secretes a detectable level of IFN-α in response to CpG-A. Thus, we pretreated PBMCs for 1 h with one of the three ABL kinase inhibitors dasatinib, imatinib, and nilotinib at clinically relevant concentrations observed in blood after administration. We then added the TLR ligands to each condition and cultured PBMCs for 24 h, and concentrations of IFN-α in the supernatants were measured by ELISA (Fig. 1A). Dasatinib strongly suppressed IFN-α production by pDCs stimulated with ODN2216 as well as natural ligands, HSV-1 or influenza virus, in a dose-dependent manner, and a low concentration (10 nM) was sufficient to induce significant suppression. Imatinib and nilotinib suppressed the IFN-α production to a lesser extent, and high concentrations (5000 and 1000 nM) were necessary to exhibit substantial suppression. When we calculated absolute amounts of IFN-α secreted from a single pDC, we obtained similar results (Supporting Information Fig. 2).

We also examined the effect of dasatinib on IFN-α production by purified pDCs to exclude indirect effects from other cell types. Dasatinib suppressed the production of IFN-α by purified pDCs, whereas imatinib did so to a lesser extent (Fig. 1B), as observed with PBMCs.

Whereas CpG-A induces pDCs to produce both IFN-α and proinflammatory cytokines (TNF-α and IL-6), CpG-B induces production of TNF-α and IL-6 but only a low level of IFN-α [16]. Thus, we next examined whether dasatinib suppresses cytokine production by pDCs stimulated with ODN2216 (CpG-A) or ODN2006 (CpG-B) to compare the suppressive effect of dasatinib on the two types of CpG DNA. Dasatinib strongly suppressed production of IFN-α, TNF-α, and IL-6 induced by ODN2216 (Fig. 1C). In contrast, dasatinib significantly suppressed IFN-α and TNF-α production induced by ODN2006 only at a high concentration (100 nM), and did not suppress IL-6 production (Fig. 1C). Dasatinib reduced the frequency of pDCs bearing intracellular IFN-α and TNF-α (Supporting Information Fig. 3), excluding the possibility that dasatinib simply blocks secretion of the cytokines. In addition, dasatinib suppressed upregulation of CD86 induced by ODN2216 but not by ODN2006 (Supporting Information Fig. 4). Dasatinib also suppressed IL-6 production induced by HSV-1 and influenza virus (Supporting Information Fig. 5).

Neither dasatinib nor imatinib significantly reduced the viability of pDCs stimulated with ODN2216 or ODN2006 (Supporting Information Fig. 6).

Collectively, these data indicate that dasatinib strongly suppresses the production of IFN-α, TNF-α, and IL-6 and the expression of CD86 by pDCs stimulated with CpG-A or natural viral ligands but not with CpG-B without reducing viability.